NASA TM X-255

NASA TM X-255

TECHNICAL MEMORANDUM

X-255

PERFORMANCE OF A VARIABLE DIVERGENT-SHROUD EJECTOR NOZZLE DESIGNED FOR FLIGHT MACH NUMBERS UP TO 3.0

By Andrew J. Stofan and James R. Mihaloew

Lewis Research Center
Cleveland, Ohio

NATIONAL AERONAUTICS AND SPACE ADMINISTRATION
WASHINGTON
January 1961

NATIONAL AERONAUTICS AND SPACE ADMINISTRATION

TECHNICAL MEMORANDUM X-255

PERFORMANCE OF A VARIABLE DIVERGENT-SHROUD EJECTOR NOZZLE DESIGNED FOR FLIGHT MACH NUMBERS UP TO 3.0*

By Andrew J. Stofan and James R. Mihaloew

SUMMARY

The performance of a continuously variable ejector nozzle designed for operation at flight Mach numbers up to 3.0 was evaluated in a 0.25-scale investigation conducted on a series of fixed configurations simulating the various positions of the variable ejector nozzle. The investigation was conducted in an unheated quiescent-air test facility to determine the pumping and internal-thrust performance of the ejector. The ejector shroud had a shortened isentropic-design internal contour. The thrust performance and pumping characteristics of the ejector were determined over a range of nozzle pressure ratios from 2 to 24 while the ejector corrected weight-flow ratio was varied from 0 to 0.22.

The ejector thrust ratio varied from about 0.983 to 0.993 throughout the range of operable conditions. The pumping performance was adequate to provide sufficient secondary air for cooling purposes.

Author

INTRODUCTION

Previous investigations have shown that fixed, or semivariable (two-position), ejector nozzles will give good on-design performance for turbojet aircraft operating up to Mach numbers of about 2.0 (refs. 1 and 2) without too great a sacrifice in the off-design region of operation. Turbojet aircraft operating over a flight regime from sea-level static to Mach 3, however, will probably have substantial off-design losses if a fixed or two-position shroud ejector is used (ref. 3). A possible solution to the problem of obtaining optimum performance over such a wide range of engine operating and flight conditions is to use continuously variable ejector geometry; that is, a variable-area primary nozzle and a variable-area shroud that can be modulated independently so as to provide near-optimum geometry over the range of flight conditions.

In order to evaluate the pumping and internal-thrust performance of such a device, a 0.25-scale investigation was conducted on a simulated

*Title, Unclassified.

continuously variable ejector with a shortened, contoured shroud designed for isentropic expansion at a flight Mach number of 3.0. A series of fixed models simulating various positions of the variable ejector were tested in an unheated quiescent-air test facility that was operated over a range of nozzle pressure ratios from 2 to 24 and ejector weight-flow ratios from 0 to 0.22. The expansion ratio was varied from 1.08 to 2.05.

SYMBOLS

The following symbols are used in this report:

A area, sq in.

D diameter, in.

F thrust, lb

L length, in.

P total pressure, lb/sq ft

p static pressure, lb/sq ft

T total temperature, ^{o}R

w airflow, lb/sec

Subscripts:

e ejector exit

ej ejector

ip ideal primary

is ideal secondary

p primary

s secondary

0 exhaust plenum, or ambient

APPARATUS

Table I lists the configurations tested, as well as the geometric variables and various simulated positions of the continuously variable Mach 3 ejector nozzle. These configurations are representative of those that would be used at various flight conditions and were investigated at the following three simulated engine operating conditions: (1) maximum afterburning (configurations 1 to 4), (2) intermediate afterburning (configurations 5 to 7), and (3) nonafterburning (configurations 8 to 12). Four additional configurations (13 to 16) were investigated to determine the effect of a 30-percent increased gap height on the thrust and pumping performance of the ejector. The increase in gap height was accomplished by using smaller diameter primary nozzles combined with the same ejector shrouds that were previously used for a given engine operating condition.

An outline sketch (solid lines) and the actual coordinates of the shortened, isentropic contoured shroud when in the design intermediate-afterburning Mach 3.0 position are given in figure 1. The shroud contour was designed for this position by taking a Mach 3.0 isentropic convergent-divergent nozzle contour and increasing the radial dimensions to allow for the passage of 7-percent secondary air; the shroud was then shortened by 40 percent. Also shown in figure 1 are the approximate locations of the pivot points and the outline of the shroud in its extreme low-Mach-number closed-down position. Obviously, the shroud contour will not be "isentropic" at positions other than the Mach 3.0 design value.

The installation of a typical ejector configuration in the test facility is shown in figures 2 and 3. The ejectors were fastened to the mounting pipe, which was in turn attached to a bedplate freely suspended from four flexure rods. This entire assembly was installed in a plenum chamber. High-pressure air was supplied to the nozzle by the laboratory air-supply system, and the plenum chamber was evacuated by the laboratory exhaust system. Pressure difference across the nozzle was made possible by labyrinth seals installed around the mounting pipe. Two vent lines connected between the two labyrinth seals and the plenum chamber decreased the pressure differential across the second labyrinth seal and prevented dynamic pressures from acting on the outside of the diffuser section. Forces acting on the nozzle and mounting pipe, both external and internal, were transmitted from the bedplate through a flexure-supported bell crank and linkage to a balanced, air-pressure-diaphragm, force-measuring cell. This entire system, which includes inlet pipe, labyrinth seals, secondary-air hose connection, air-measuring station, and force-measuring cell, was calibrated before the ejectors were installed.

CJ-1 back

INSTRUMENTATION

Pressures and temperatures were measured at various stations as shown in figure 2 and in the following table:

Station	Total-pressure tubes	Static-pressure taps	Temperature thermocouples
0 - Exhaust plenum	--	4	2
1 - Mounting-pipe inlet	--	4	2
2 - Airflow	12	8	-
3 - Primary-nozzle inlet	8	4	2
4 - Secondary-air passage	12	-	-
Secondary-air orifice	--	2	2

Pressures obtained from total-pressure rakes and wall static-pressure taps at stations 1 and 2 were used in the computation of inlet momentum and airflow. Total-pressure and total-temperature rakes were installed at station 3 to determine nozzle-inlet conditions, and at station 4 to measure secondary total pressure. Station 0 was used to measure plenum-chamber static pressure and temperature. The secondary flow was measured by a flat-plate orifice, two static-pressure taps, and two thermocouples located in the secondary-air line.

PROCEDURE

The testing procedure for each configuration was the same. A range of ejector corrected weight-flow ratios ($(w_s/w_p)\sqrt{T_s/T_p}$, where T_s/T_p = 1.0 for this investigation) from 0 to 0.22 was covered; and, at various nominal values of corrected weight-flow ratio, the nozzle pressure ratio P_p/p_0 was varied from 2 to 24. The ejector schedule illustrated in figure 4 outlines the primary-nozzle area ratio as a function of expansion ratio for the configurations investigated.

The measured axial thrust was determined from summing up the pertinent forces acting on the nozzle - mounting-pipe system. The ideal ejector thrust was calculated from the measured primary and secondary mass flows, with isentropic expansion assumed from the respective measured total pressures to ambient. The thrust ratio is defined as the measured axial thrust divided by the sum of the ideal primary and secondary thrusts. The flow coefficient is the ratio of the actual mass flow divided by the ideal mass flow. A more detailed explanation of the methods of calculation of the thrust ratio and flow coefficient is given in reference 4.

RESULTS AND DISCUSSION

Primary-Nozzle Performance

The performance of the primary nozzles is shown in figure 5. The thrust performance for the five primary nozzles is nearly the same, whereas the flow coefficient in figure 5(b) decreases about four points as the nozzle convergence angle increases from about 14° to 36°.

Ejector Performance

The basic performance of the ejector configurations, as a function of primary pressure ratio, is shown in figures 6 to 21 and includes the thrust ratio and pumping characteristics for a range of ejector corrected weight-flow ratios from 0 to 0.22.

Examination of the thrust curves in figures 6 to 21 shows that, in the maximum thrust region of each configuration, the thrust ratio is relatively insensitive to primary pressure ratio. To illustrate this insensitivity, the range of primary pressure ratios over which the thrust is within 1/4 percent of the maximum value is presented as a function of expansion ratio in figure 22 for a range of ejector corrected weight-flow ratios between 0.04 and 0.11. Performance parameters for the configurations investigated are discussed in terms of this region of primary pressure ratio at which near maximum thrust ratio occurred. In addition, in order to better understand the relation between ejector performance and flight-plan requirements, a schedule of primary-nozzle pressure ratio and inlet performance characteristics (based on an inlet kinetic-energy efficiency of 95 percent) with flight Mach number has been assumed and is used as a basis for discussion. This schedule, which is based on the performance of a hypothetical Mach 3.0 turbojet aircraft, is shown in figure 23.

The variation of thrust ratio with primary pressure ratio and approximate flight Mach number for the three simulated engine operating conditions is shown in the composite-thrust-performance curves in figure 24. Each curve is indicative of the performance that would be obtained with a continuously variable ejector. Data are presented for ejector corrected weight-flow ratios of 0.04 and 0.11. The thrust ratio for the three operating conditions is very nearly constant over the range of primary-nozzle pressure ratios investigated and shows a variation only between 0.983 and 0.993. The figure also indicates that the ejector design thrust ratio is insensitive to ejector corrected weight-flow ratios between 0.04 and 0.11. Although the ejector thrust performance for the isentropic contoured shroud is quite high, it is felt that the thrust performance of an ejector nozzle with a conical shroud and the same L/D and diameter ratios would be practically as good.

The composite pumping performance associated with the thrust performance of figure 24 is shown in figure 25 for the same three operating conditions. The curve of maximum ejector pressure ratio P_s/P_p available was based on the assumed flight schedule (fig. 23) plus an assumed subsonic-duct total-pressure recovery of 0.95. Figure 25 indicates that at the most critical operating condition (P_p/p_0 = 4 to 5) at least 6 percent corrected secondary flow can be supplied and, at both higher and lower pressure ratios, greater amounts than this are obtainable.

Primary-Nozzle Flow Performance (With Shrouds)

The composite primary-nozzle flow performance (for the same operating conditions as the two previous figures) with the ejector shroud in place is shown in figure 26 for three different values of $(w_s/w_p)\sqrt{T_s/T_p}$. It is apparent that the primary-nozzle flow coefficient is reduced by higher ejector weight-flow ratios when the shroud is in place. This drop in flow coefficient is due to the increased secondary flow requiring additional space, thereby unchoking the primary nozzle at its exit; this, in turn, lowers the flow coefficient (ref. 5).

Effect of Increased Gap Height on Performance

The thrust and pumping performance for the configurations with a 30-percent increase in gap height are shown in figures 18 to 21. These four configurations, 13, 14, 15, and 16, are comparable with and would operate in the same region as configurations 9, 12, 2, and 4, respectively. A comparison of the performance of corresponding configurations indicates that an increase of about 18 percent in pumping capacity was obtained with the increased gap configurations without noticeable lowering of the thrust performance; that is, 18-percent-less ejector pressure ratio P_s/P_p is required to provide the same ejector corrected weight-flow ratio $(w_s/w_p)\sqrt{T_s/T_p}$. These data are included only to show the performance for an increased gap height and are not discussed elsewhere.

SUMMARY OF RESULTS

A small-scale performance investigation was conducted on a series of configurations that simulated various positions of a continuously variable ejector nozzle designed with an isentropic-type contoured shroud for operation at flight Mach numbers up to 3.0. Results indicated that:

1. The ejector thrust ratio was very nearly constant over the range of primary-nozzle pressure ratios investigated, showing a variation between 0.983 and 0.993. The ejector thrust ratio was insensitive to variations in ejector corrected weight-flow ratios between 0.04 and 0.11.

2. The pumping performance indicated that most cooling requirements can probably be satisfied.

3. An increase of 30 percent in gap height between primary nozzle and shroud resulted in an increase of 18 percent in pumping capacity without lowering the thrust performance.

E-736

Lewis Research Center
National Aeronautics and Space Administration
Cleveland, Ohio, February 8, 1960

REFERENCES

1. Mihaloew, James R.: Internal-Performance Evaluation of a Fixed-Divergent-Shroud Ejector. NASA TN D-763, 1960.

2. Mihaloew, James R. and Stofan, Andrew J.: Internal-Performance Evaluation of a Two-Position Divergent-Shroud Ejector. NASA TN D-762, 1960.

3. Beheim, Milton A.: Off-Design Performance of Divergent Ejectors. NACA RM E58G10a, 1958.

4. Trout, Arthur M., Papell, S. Stephen, and Povolny, John H.: Internal Performance of Several Divergent-Shroud Ejector Nozzles with High Divergence Angles. NACA RM E57F13, 1957.

5. Kochendorfer, Fred D.: Note on Performance of Aircraft Ejector Nozzles at High Secondary Flows. NACA RM E54F17a, 1954.

TABLE I. - EJECTOR CONFIGURATIONS AND GEOMETRIC VARIABLES

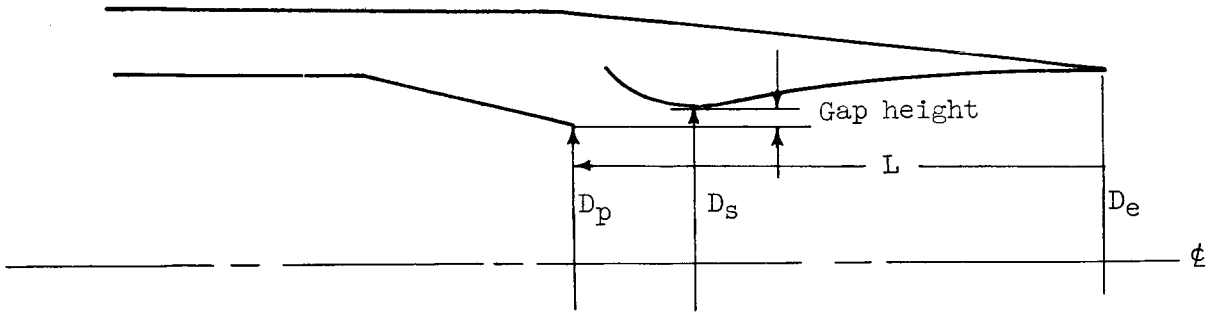

Configuration	Geometric variables				Simulated engine operating condition	
	D_p, in.	D_e/D_p	L/D_p	D_s/D_p	Afterburning	Mach number
1	8.23	1.08	1.38	1.09	Maximum	Sea-level static
2	↓	1.16	1.39	1.11	↓	0.9
3		1.34	1.40	1.10		1.5
4		1.54	1.41	1.10		2.2
5	7.46	1.08	1.53	1.08	Intermediate	Sea-level static
6	↓	1.34	1.56	1.11	↓	1.5
7		1.73	1.57	1.12		2.6 to 3.0
8	6.62	1.08	1.74	1.09	None	Sea-level static
9	↓	1.16	1.75	1.10	↓	0.9
10		1.34	1.78	1.11		1.5
11		1.54	1.79	1.13		2.2
12		1.97	1.81	1.15		3.0
13	6.37	1.21	1.84	1.14	None: 30% increase in gap height	0.9
14	6.37	2.05	1.88	1.20		3.0
15	7.98	1.20	1.44	1.14	Maximum: 30% increase in gap height	0.9
16	7.98	1.59	1.46	1.14		2.2

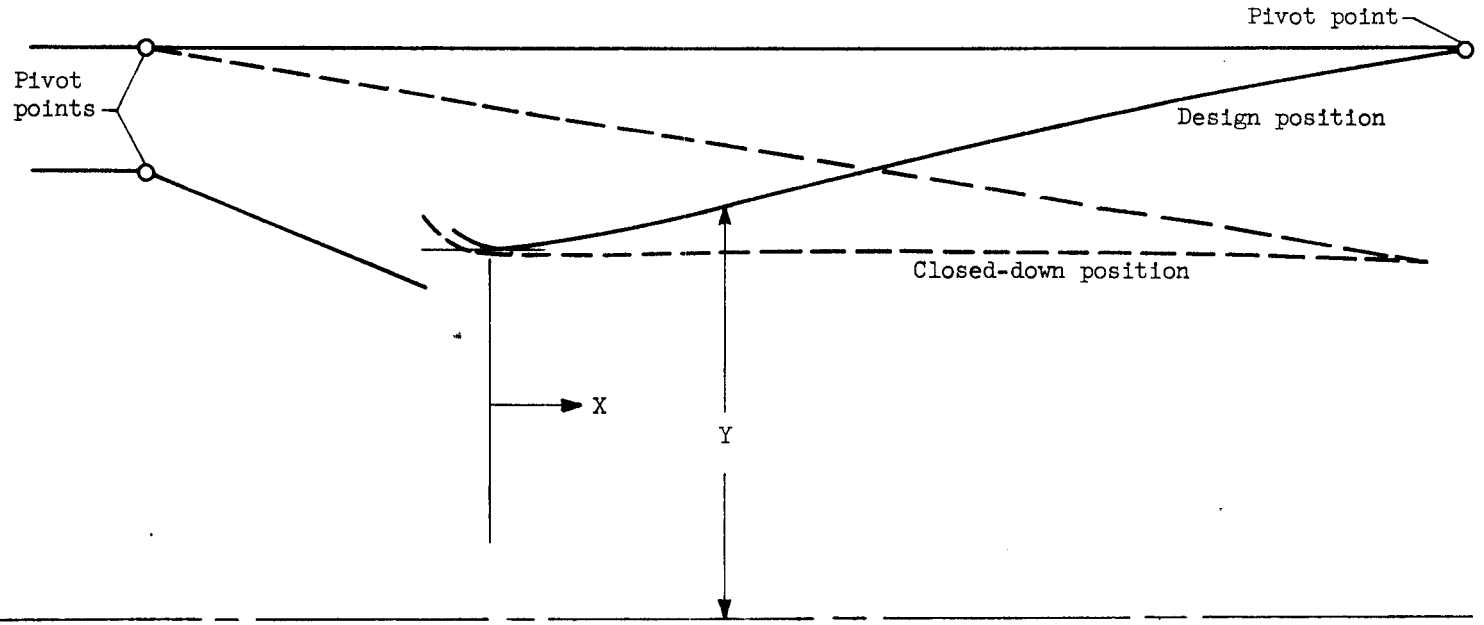

Coordinates	
X/D_p	Y/D_p
0	0.560
.109	.573
.310	.617
.511	.669
.712	.716
.913	.764
1.114	.803
1.315	.838
1.472	.865

Figure 1. - Design coordinates for isentropic-design shroud. Intermediate afterburning, Mach 2.6 to 3.0 position.

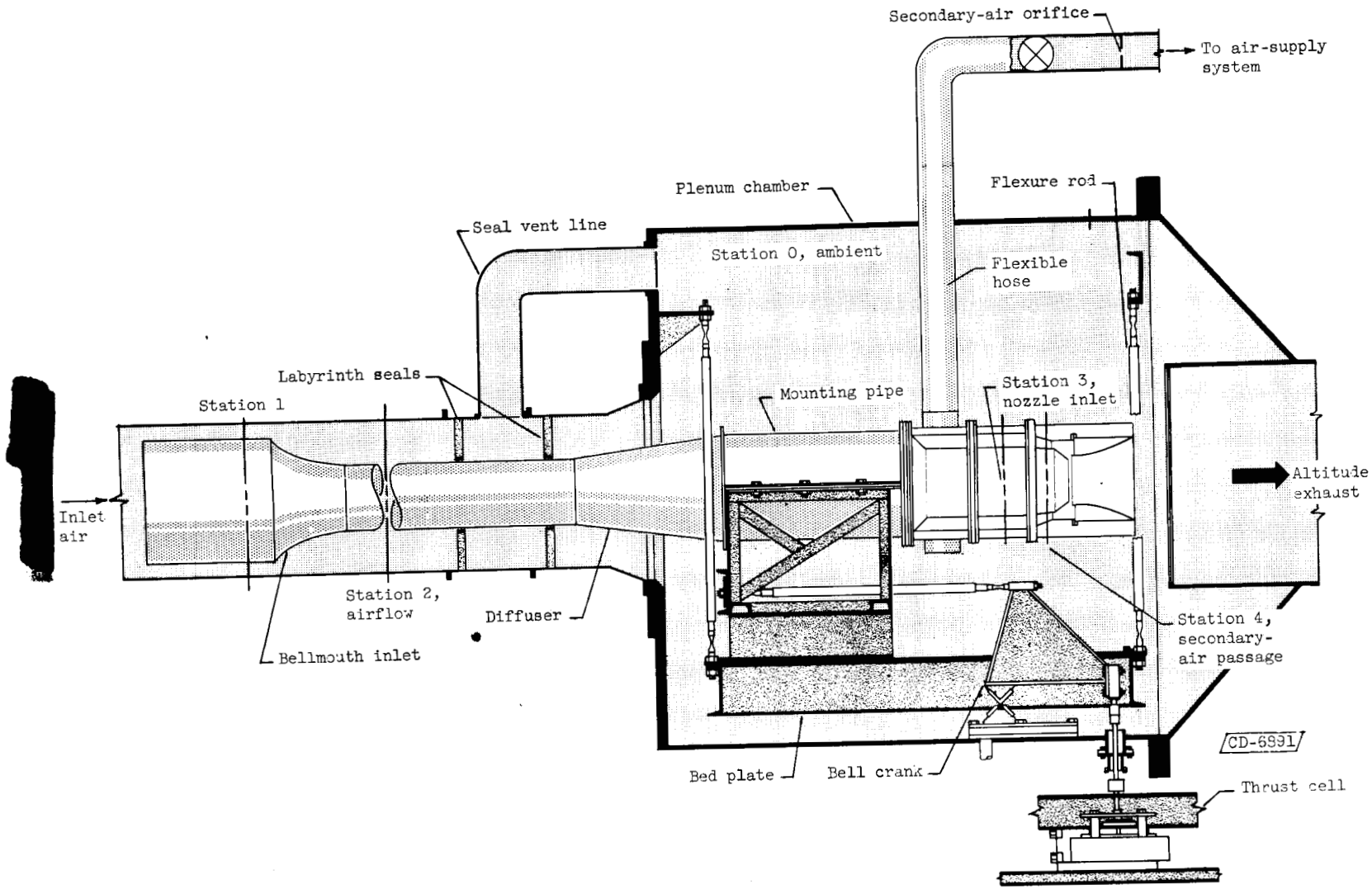

Figure 2. - Ejector test facility.

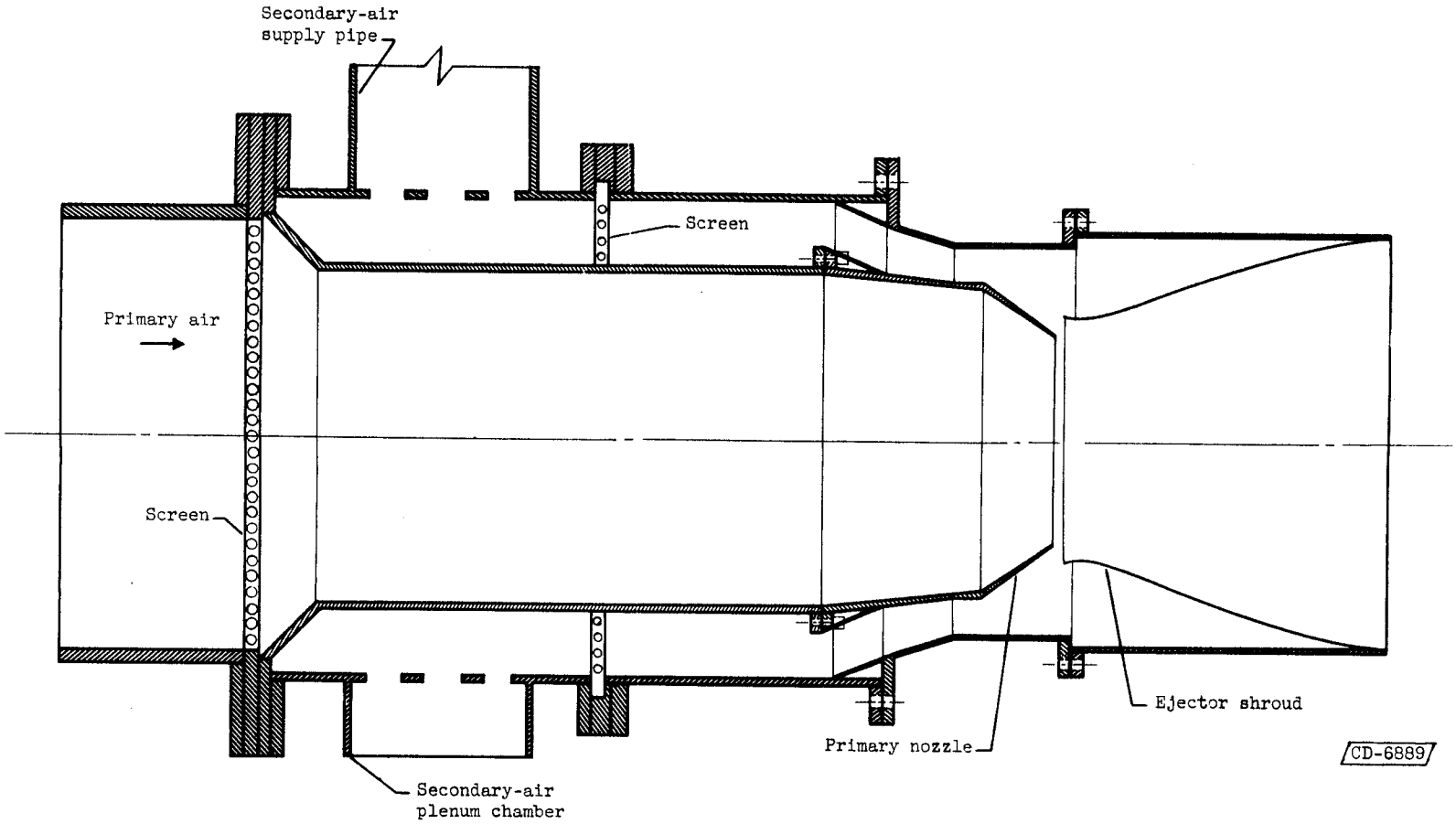

Figure 3. - Ejector installation.

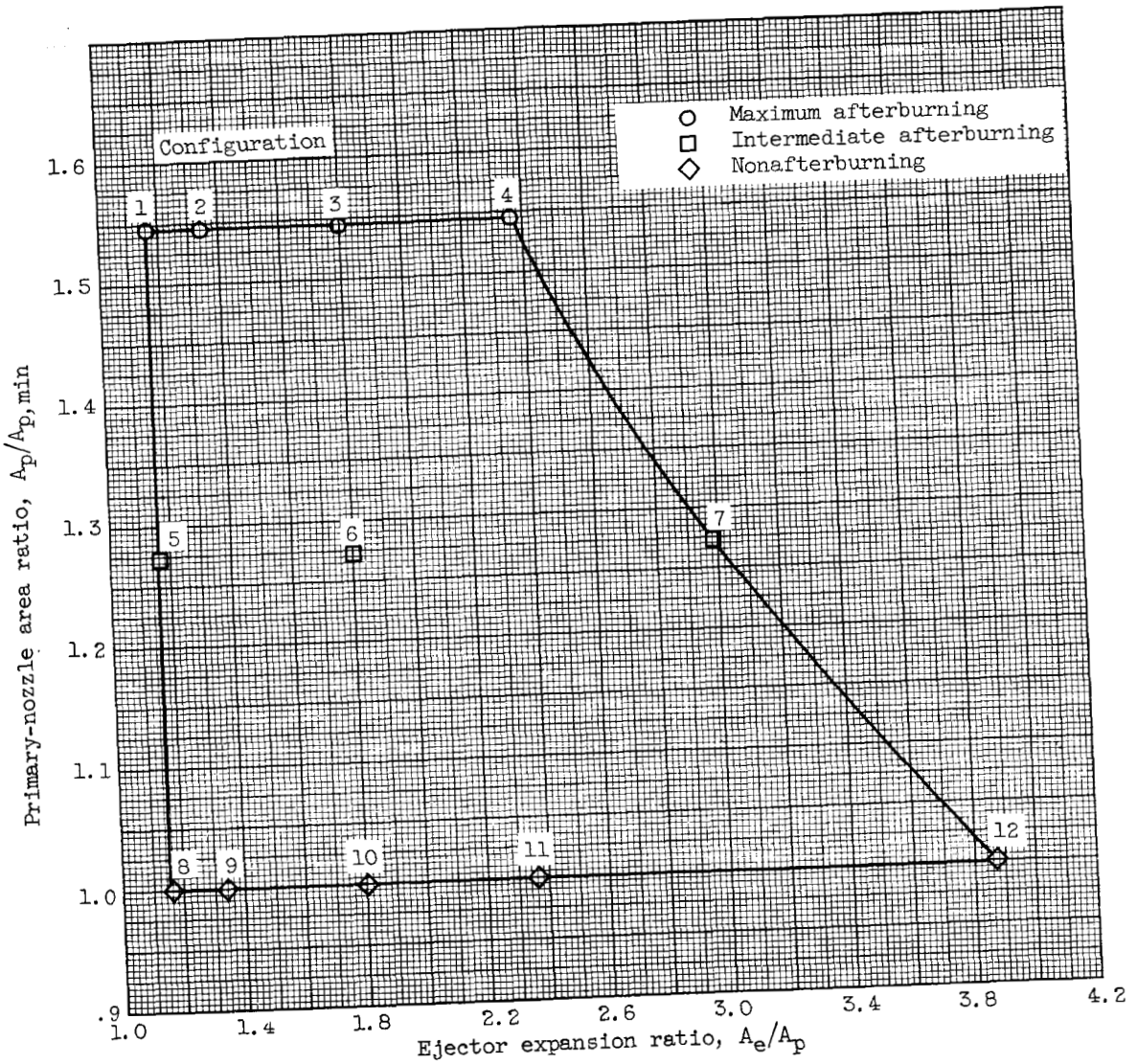

Figure 4. - Ejector schedule.

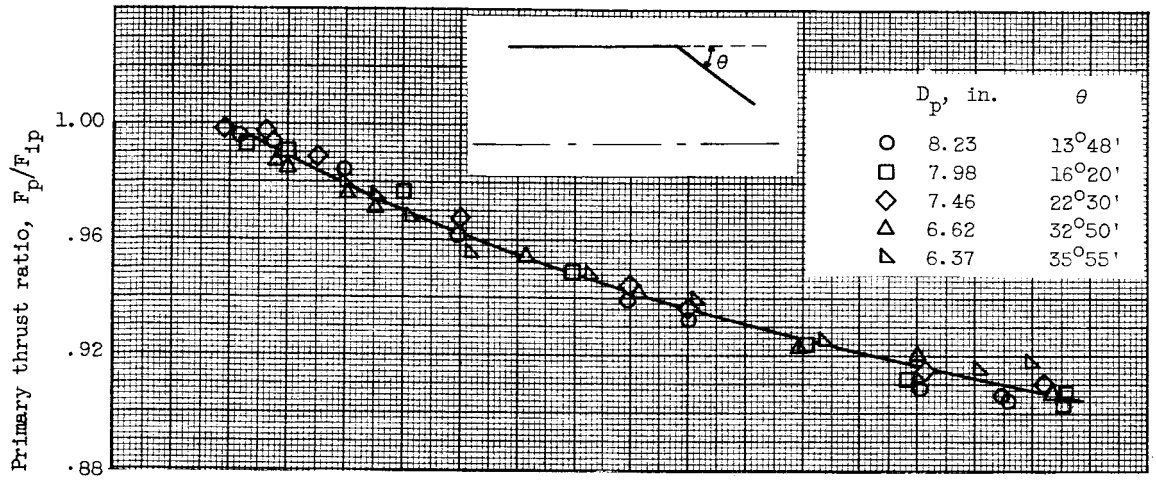

(a) Thrust performance.

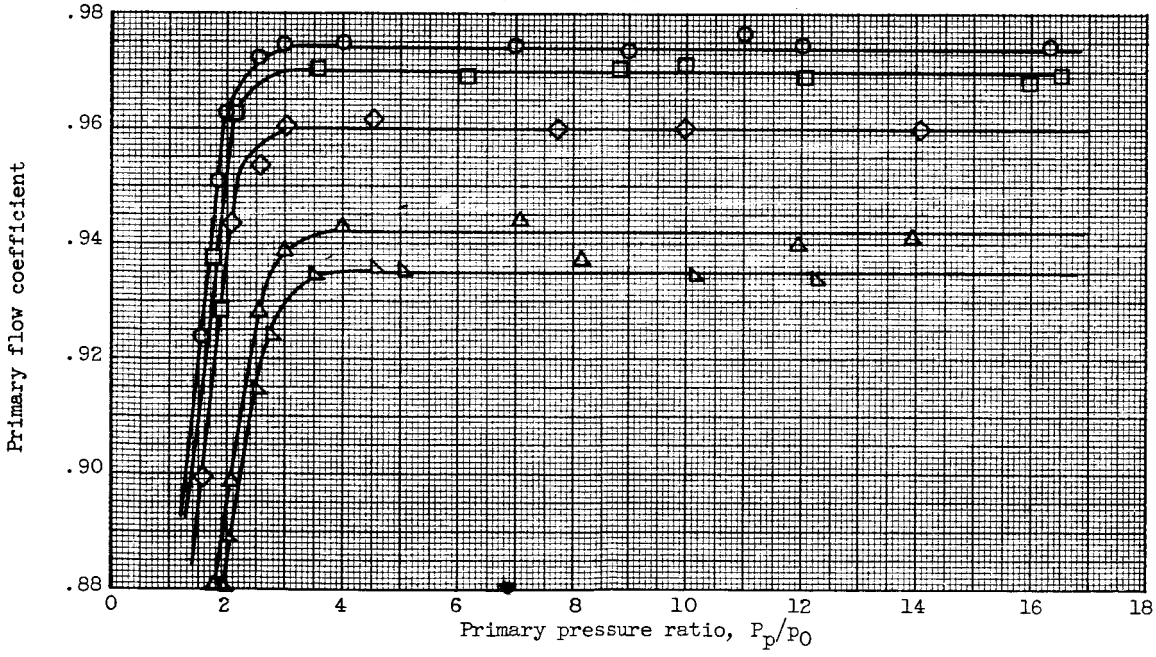

(b) Flow performance.

Figure 5. - Primary-nozzle performance (without shrouds).

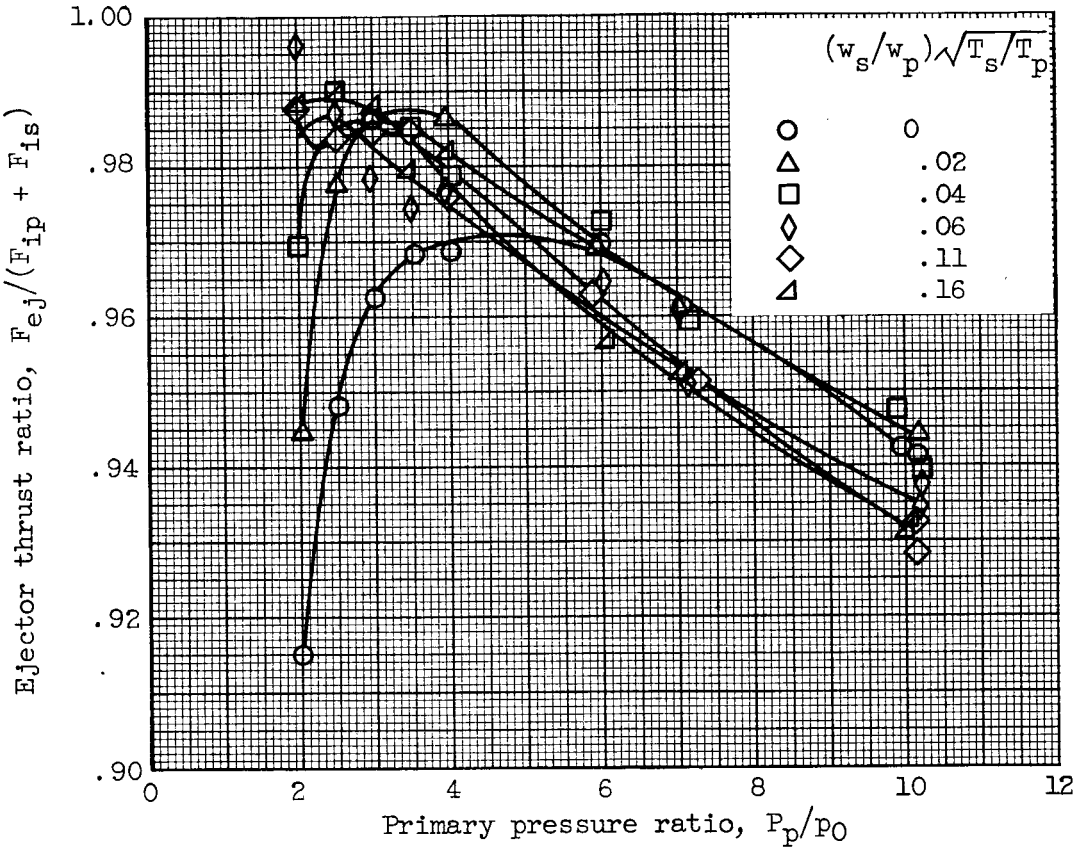

(a) Thrust performance.

Figure 6. - Ejector performance for configuration 1, which simulates position for maximum afterburning, sea-level static.

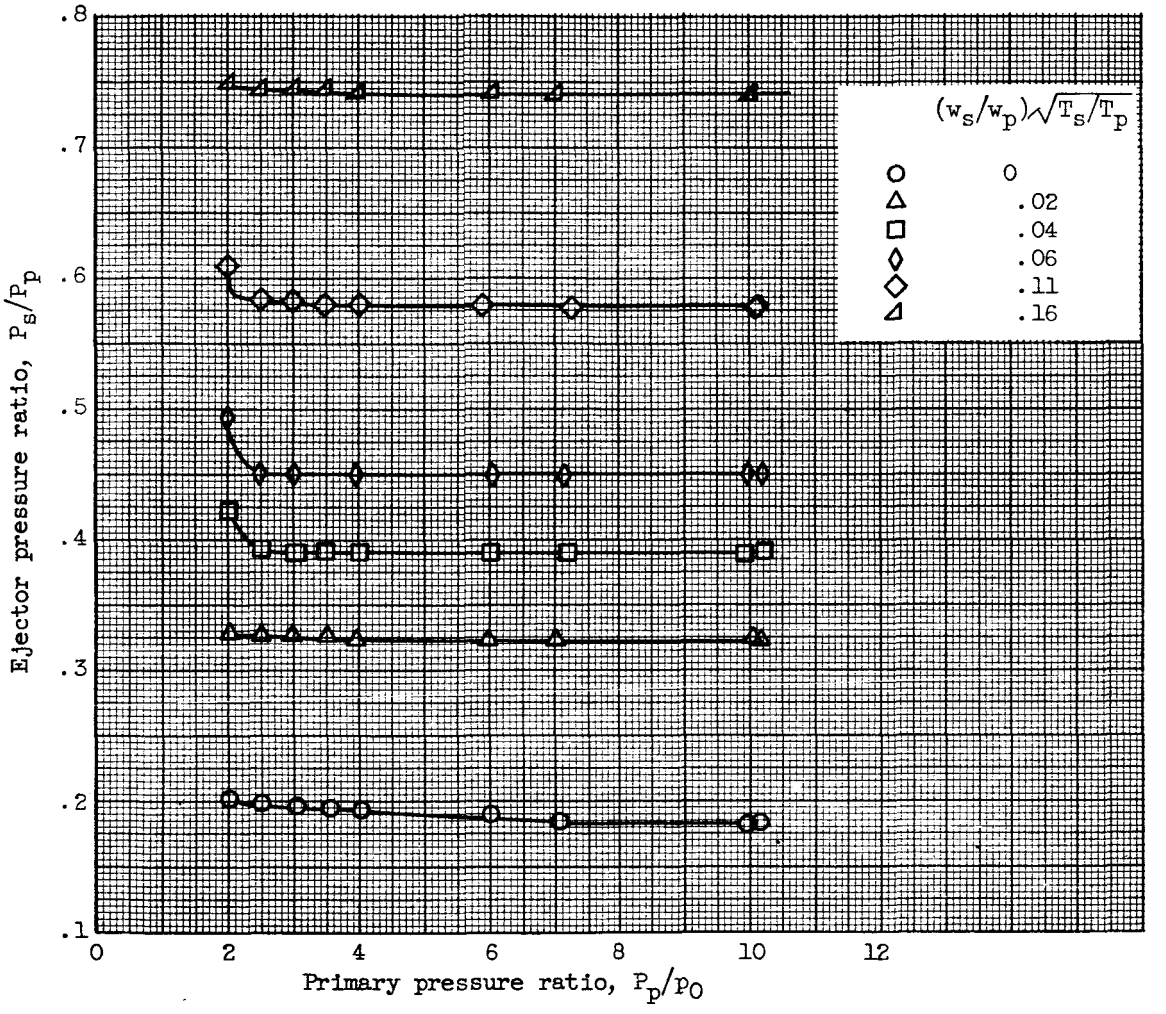

(b) Pumping performance.

Figure 6. - Concluded. Ejector performance for configuration 1, which simulates position for maximum afterburning, sea-level static.

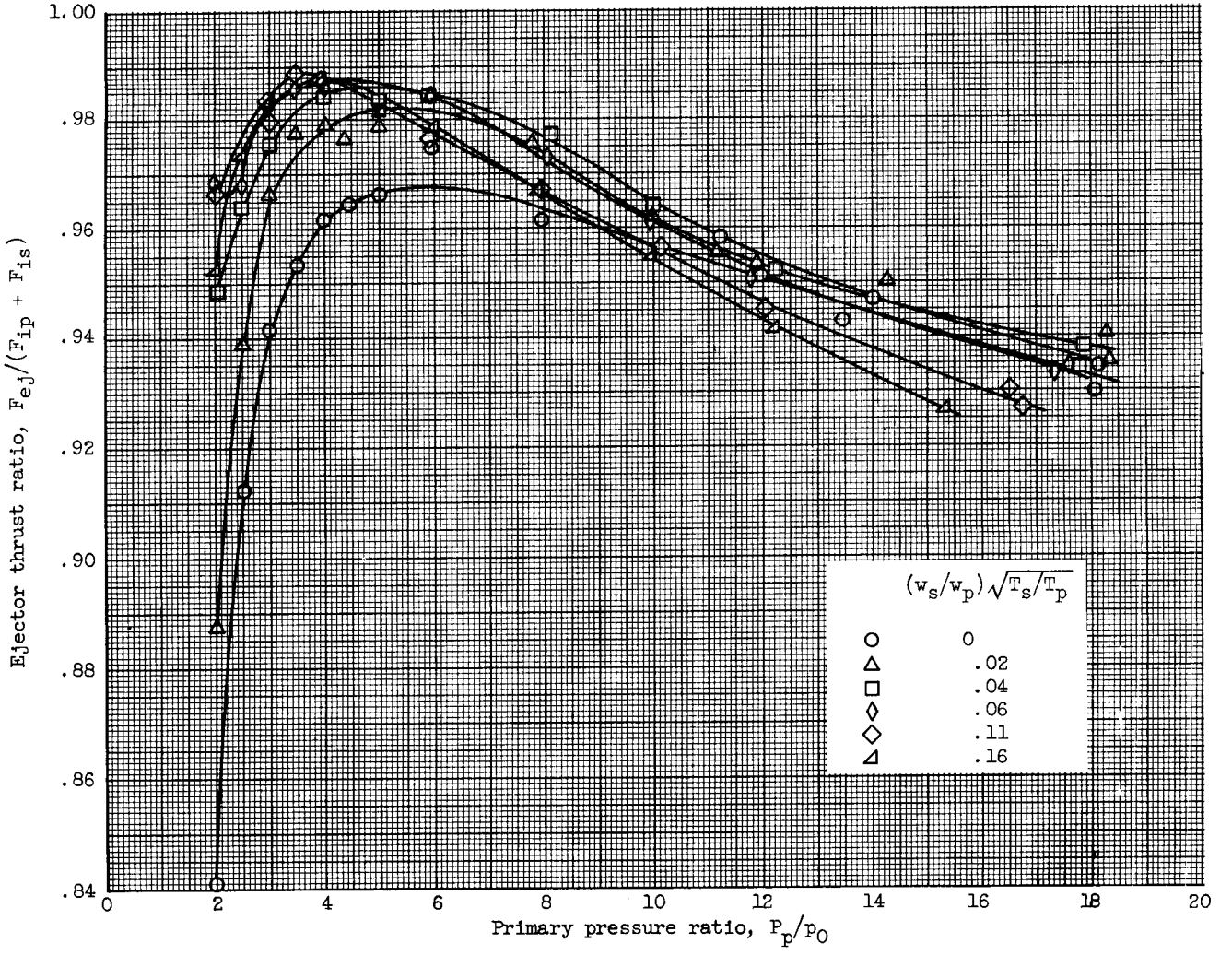

(a) Thrust performance.

Figure 7. - Ejector performance for configuration 2, which simulates position for maximum afterburning, Mach 0.9.

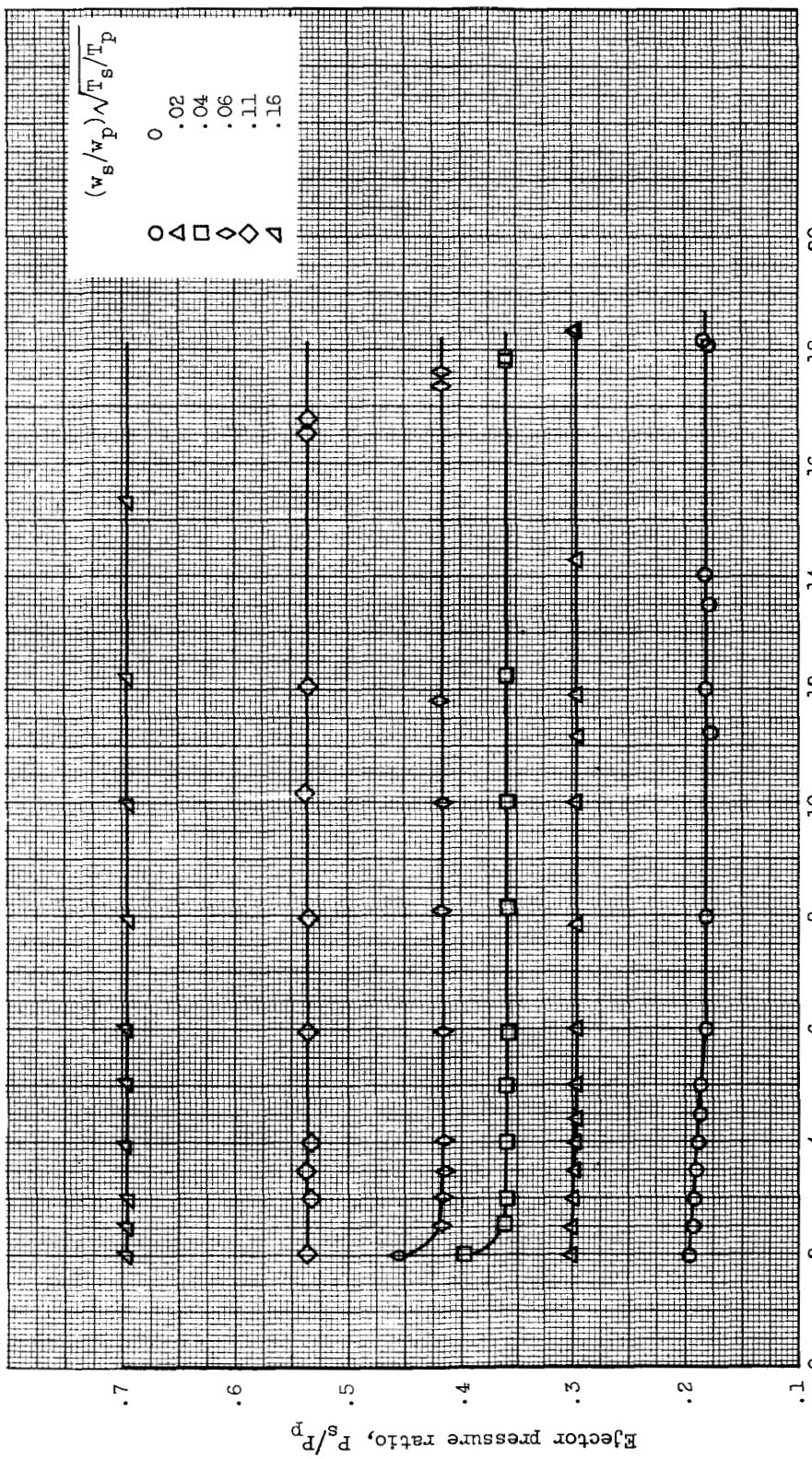

(b) Pumping performance.

Figure 7. - Concluded. Ejector performance for configuration 2, which simulates position for maximum afterburning, Mach 0.9.

E-756

CU-3

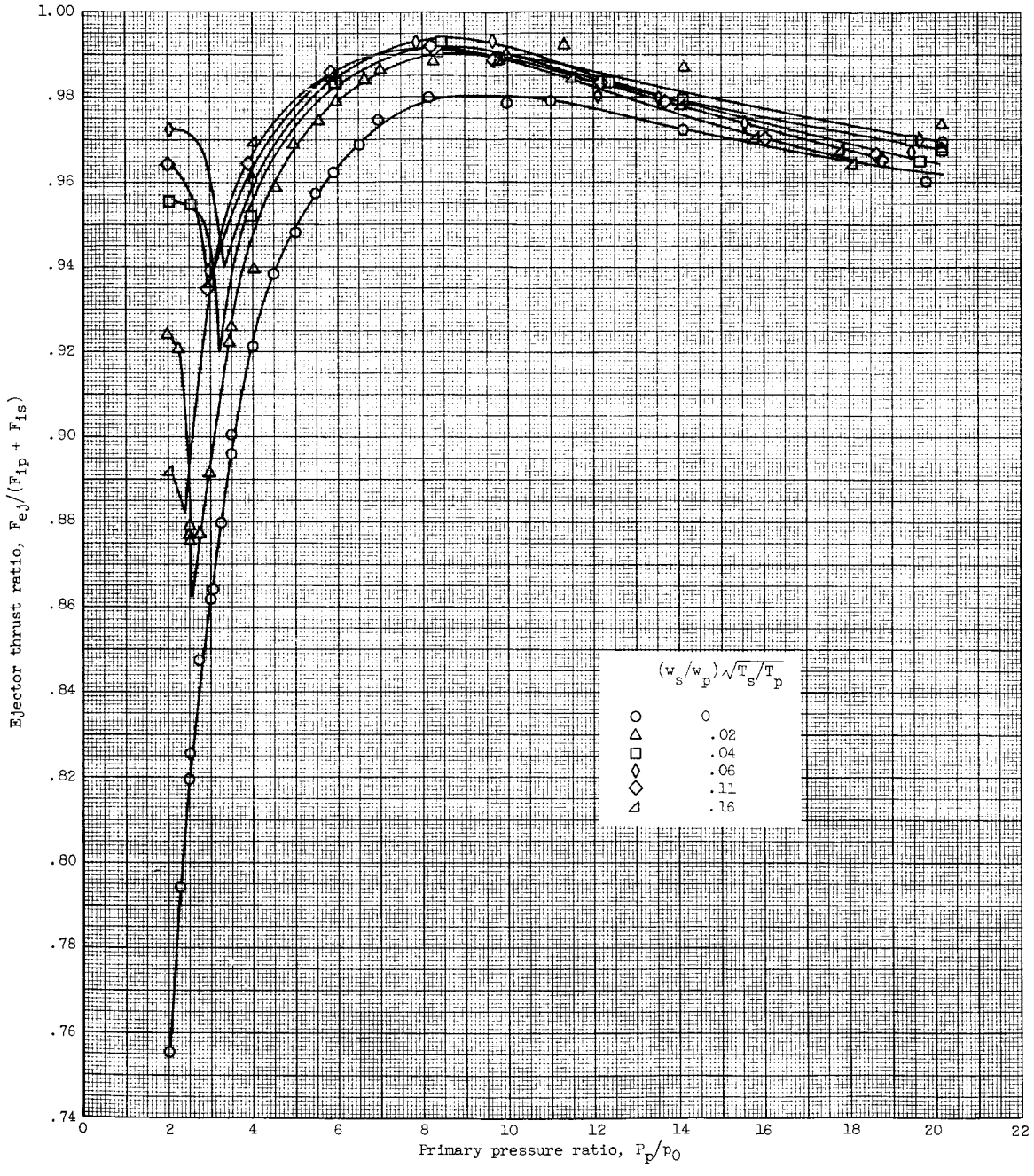

(a) Thrust performance.

Figure 8. - Ejector performance for configuration 3, which simulates position for maximum afterburning, Mach 1.5.

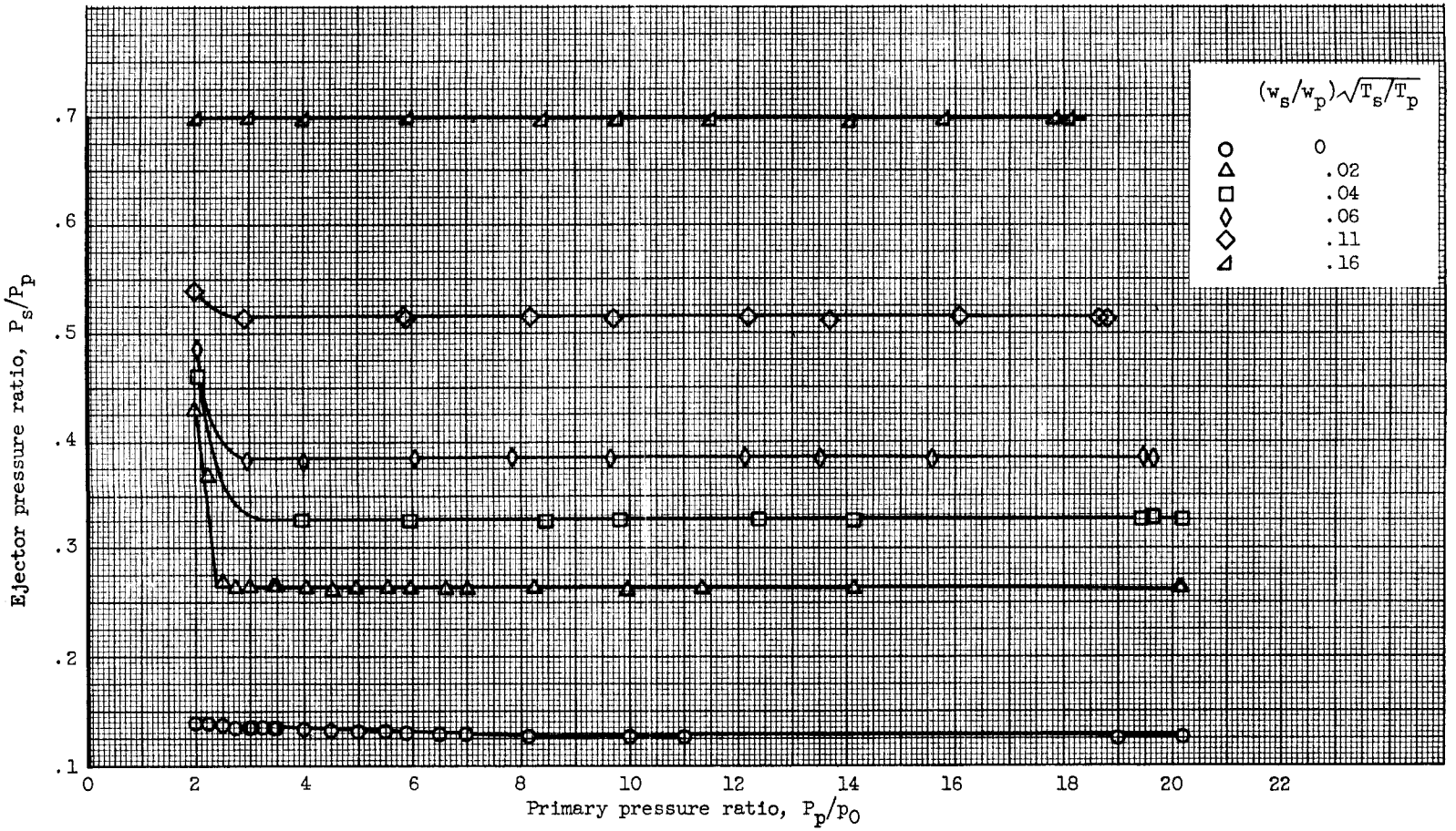

(b) Pumping performance.

Figure 8. - Concluded. Ejector performance for configuration 3, which simulates position for maximum afterburning, Mach 1.5.

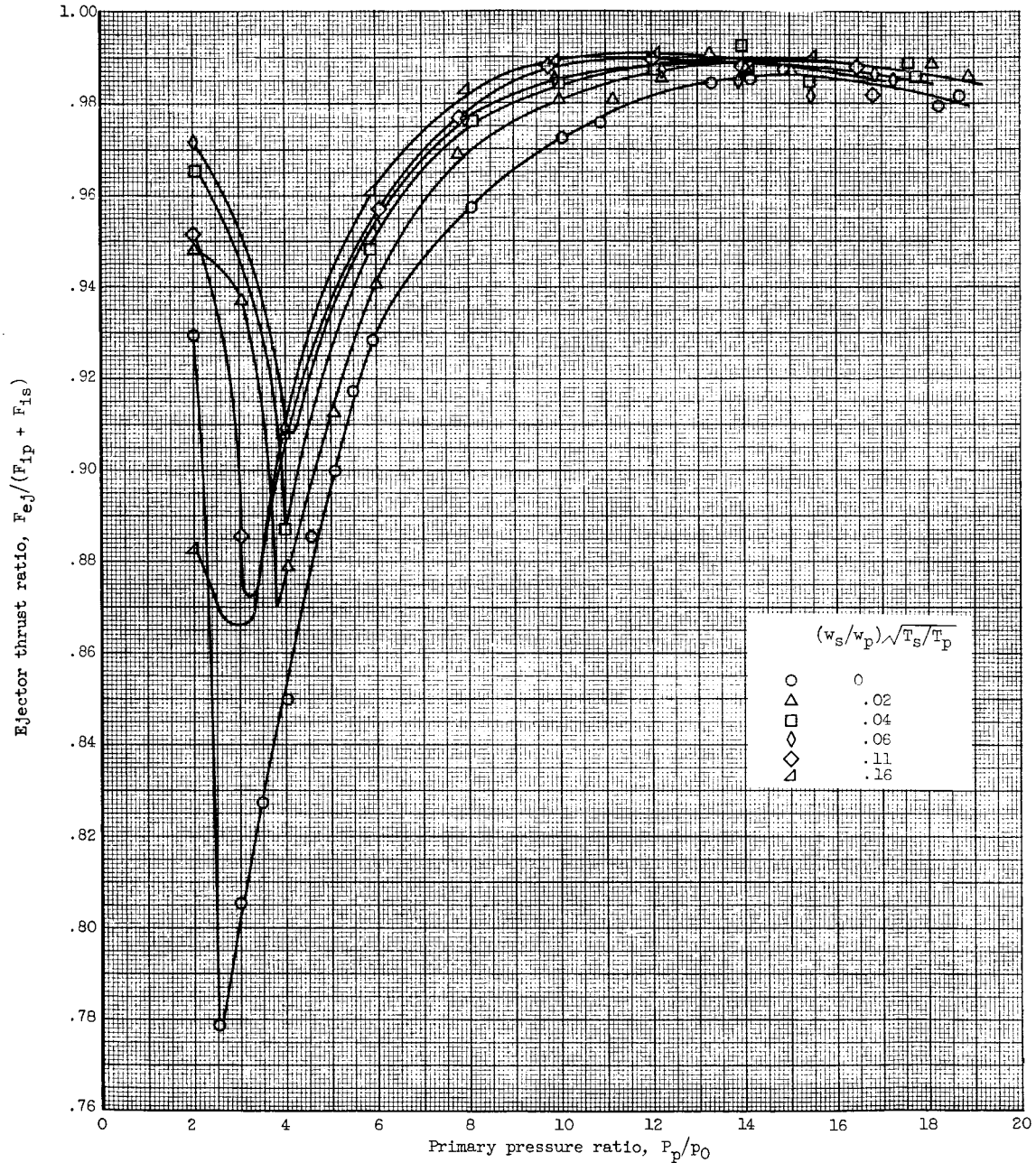

(a) Thrust performance.

Figure 9. - Ejector performance for configuration 4, which simulates position for maximum afterburning, Mach 2.2.

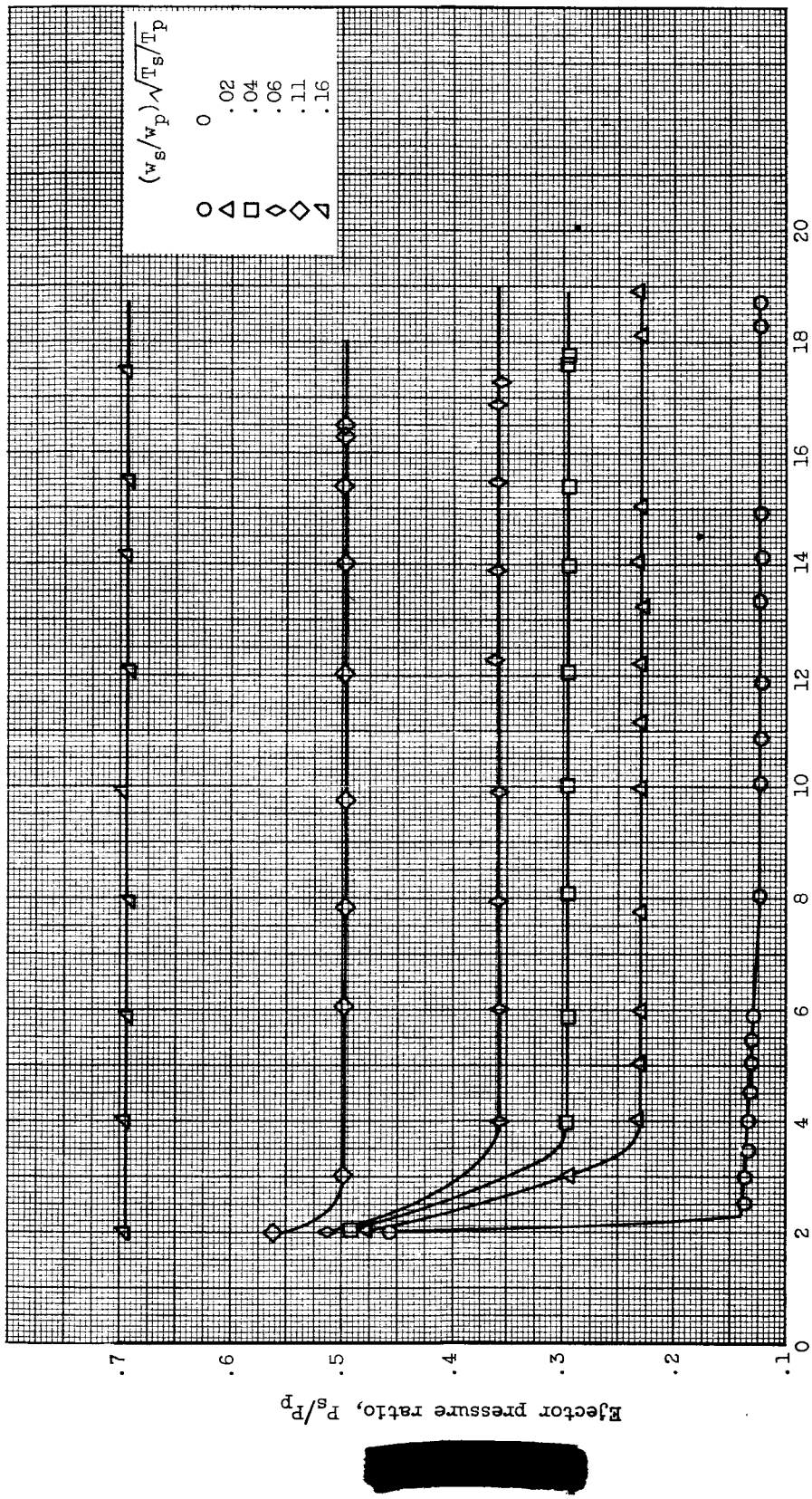

(b) Pumping performance.

Figure 9. - Concluded. Ejector performance for configuration 4, which simulates position for maximum afterburning, Mach 2.2.

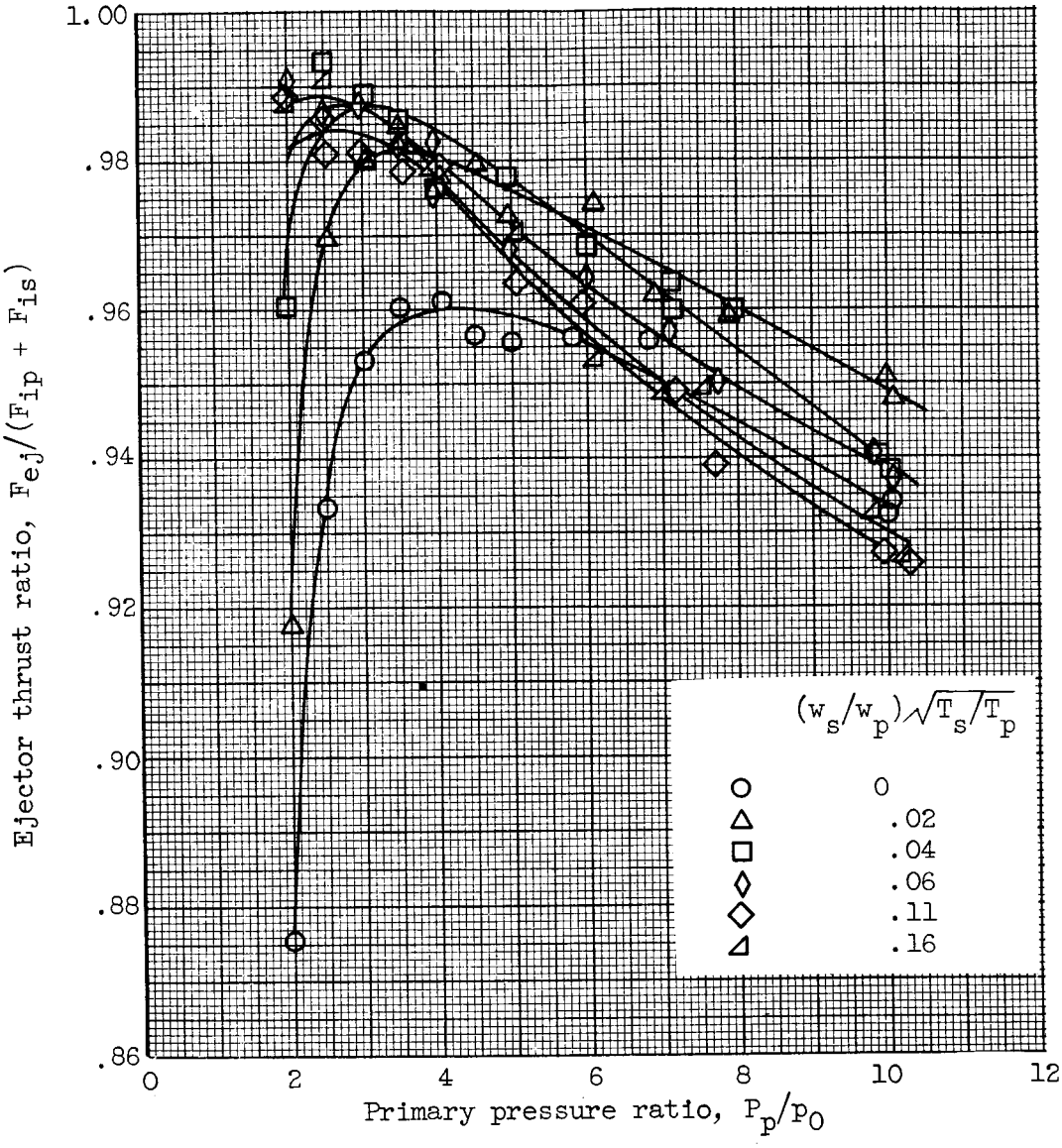

(a) Thrust performance.

Figure 10. - Ejector performance for configuration 5, which simulates position for intermediate afterburning, sea-level static.

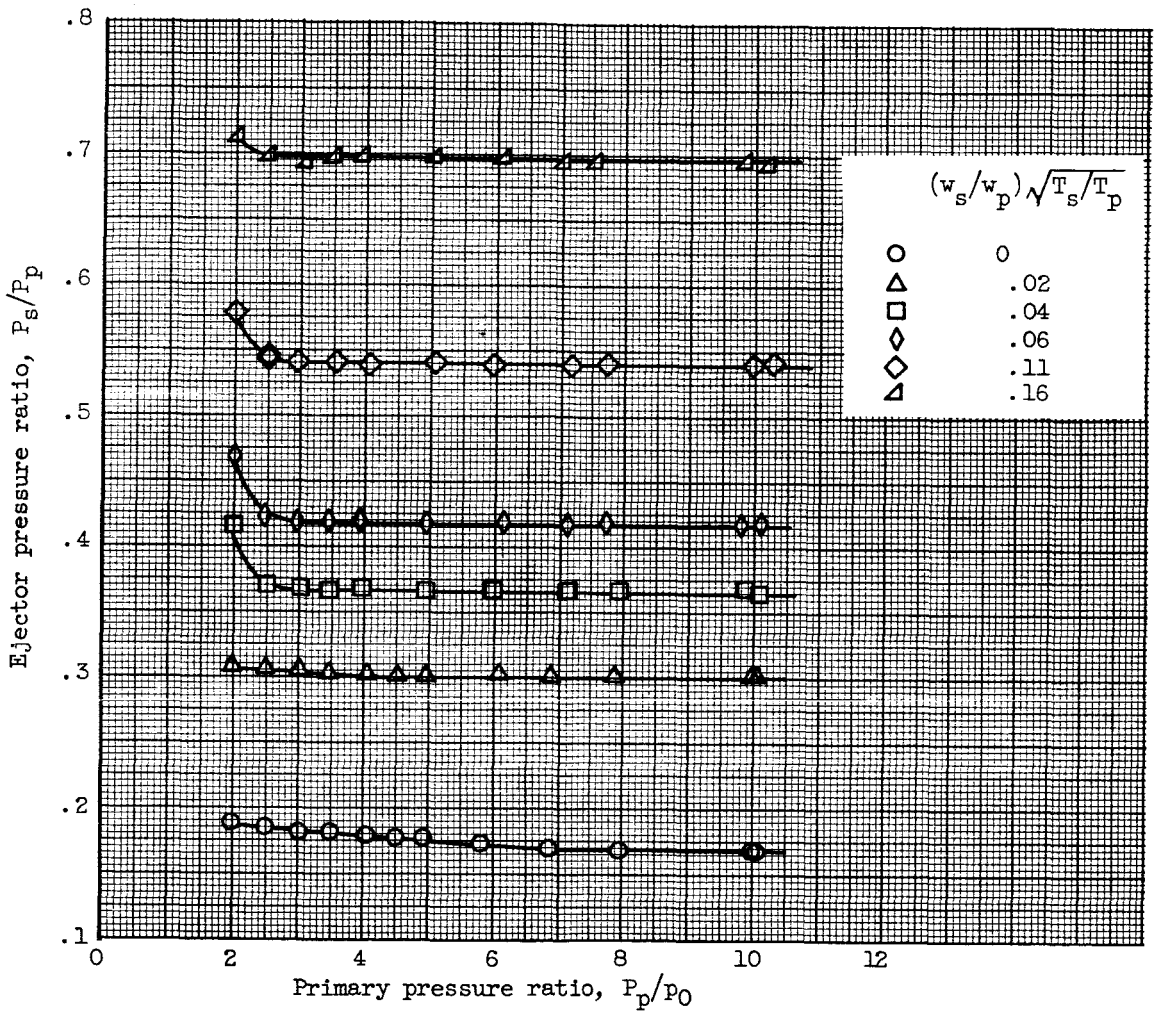

(b) Pumping performance.

Figure 10. - Concluded. Ejector performance for configuration 5, which simulates position for intermediate afterburning, sea-level static.

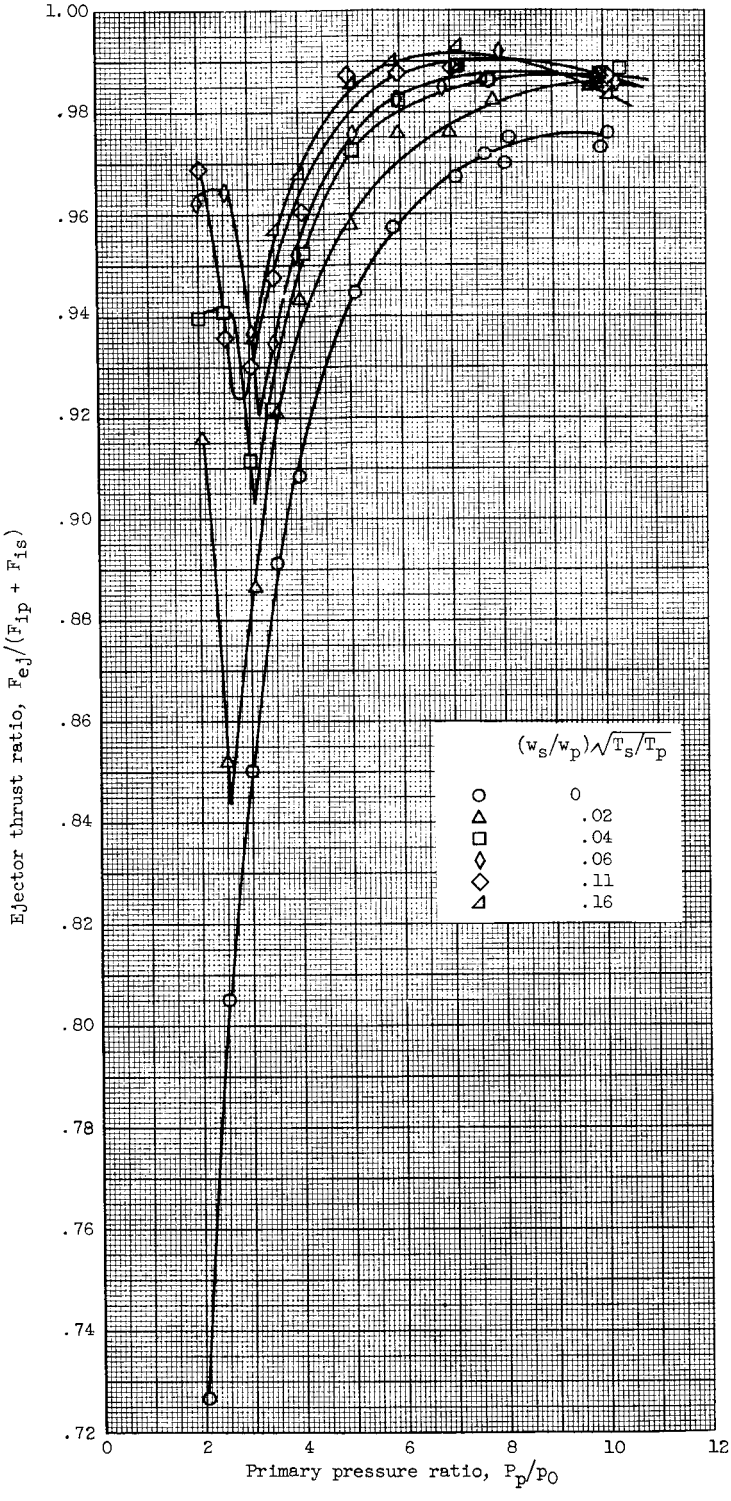

(a) Thrust performance.

Figure 11. - Ejector performance for configuration 6, which simulates position for intermediate afterburning, Mach 1.5.

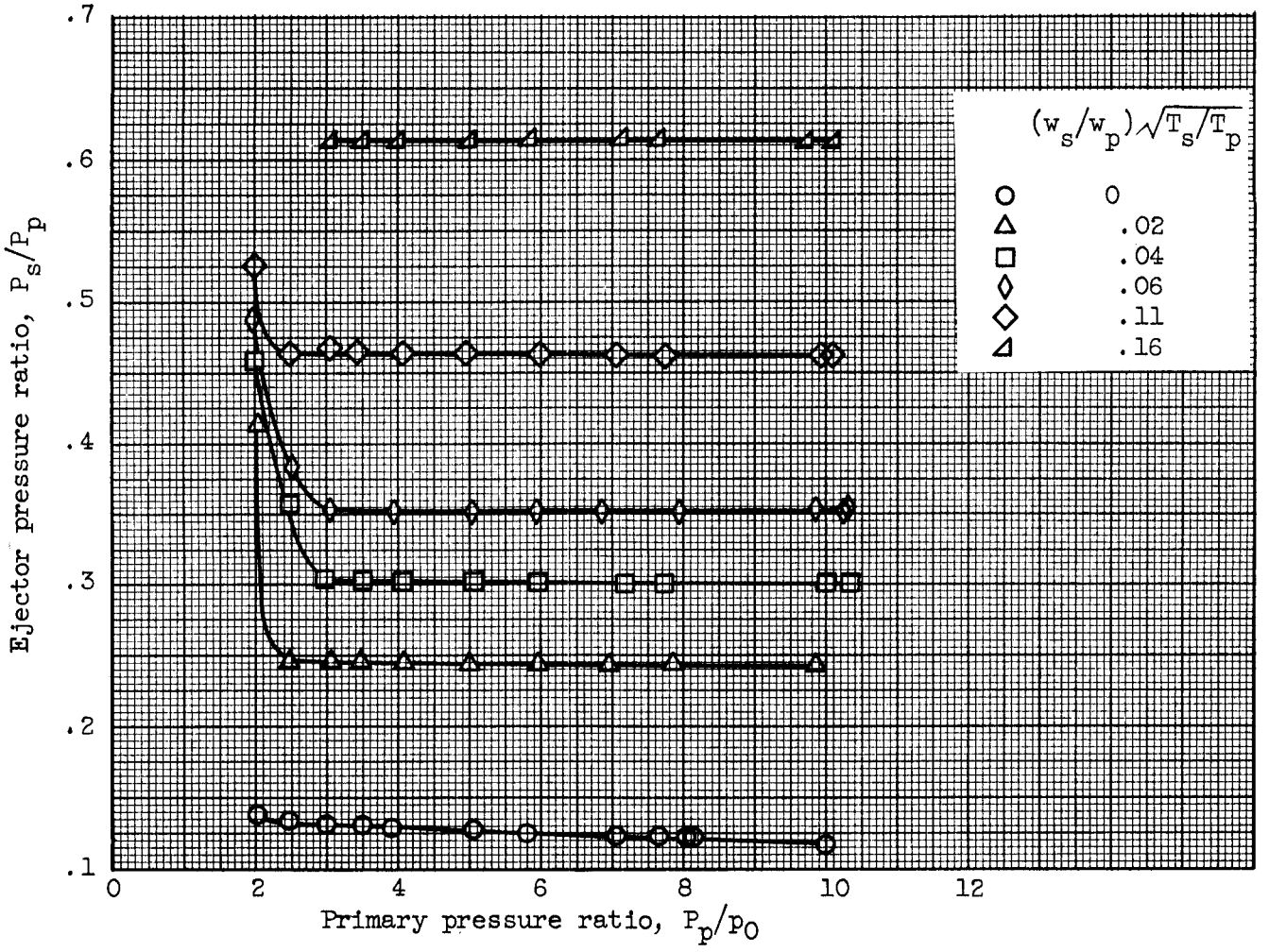

(b) Pumping performance.

Figure 11. - Concluded. Ejector performance for configuration 6, which simulates position for intermediate afterburning, Mach 1.5.

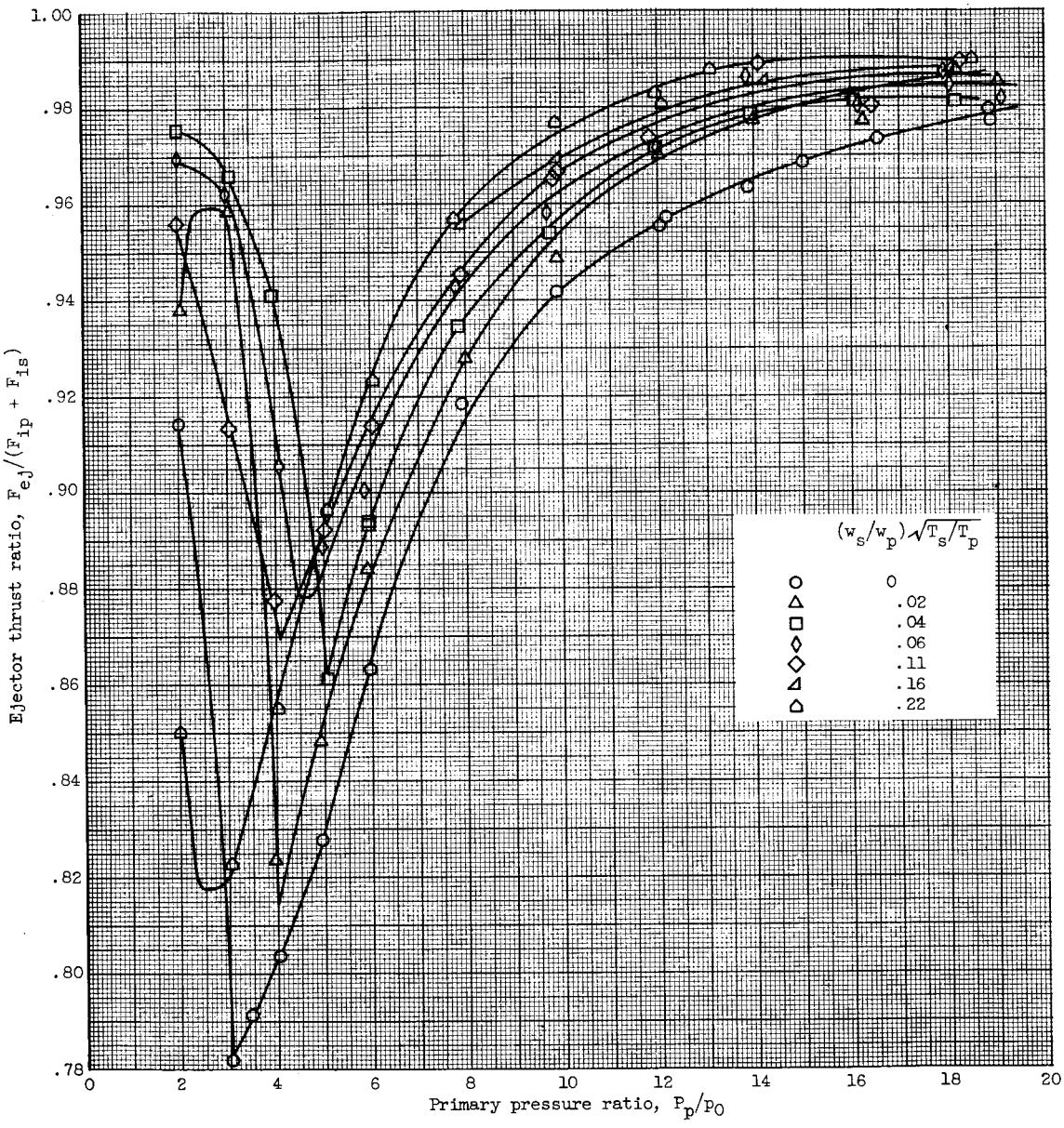

(a) Thrust performance.

Figure 12. - Ejector performance for configuration 7, which simulates position for intermediate afterburning, Mach 2.6 to 3.0.

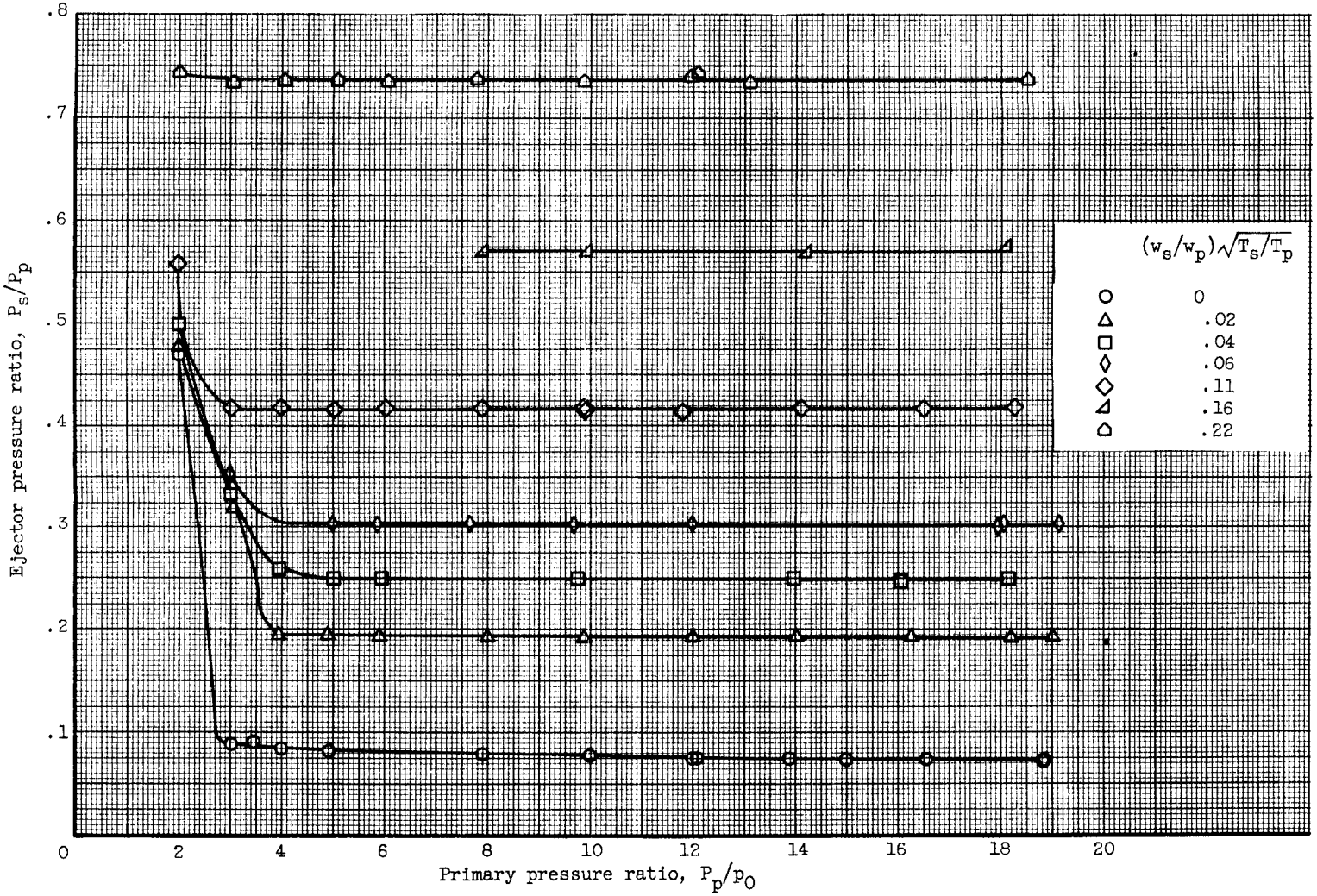

(b) Pumping performance.

Figure 12. - Concluded. Ejector performance for configuration 7, which simulates position for intermediate afterburning, Mach 2.6 to 3.0.

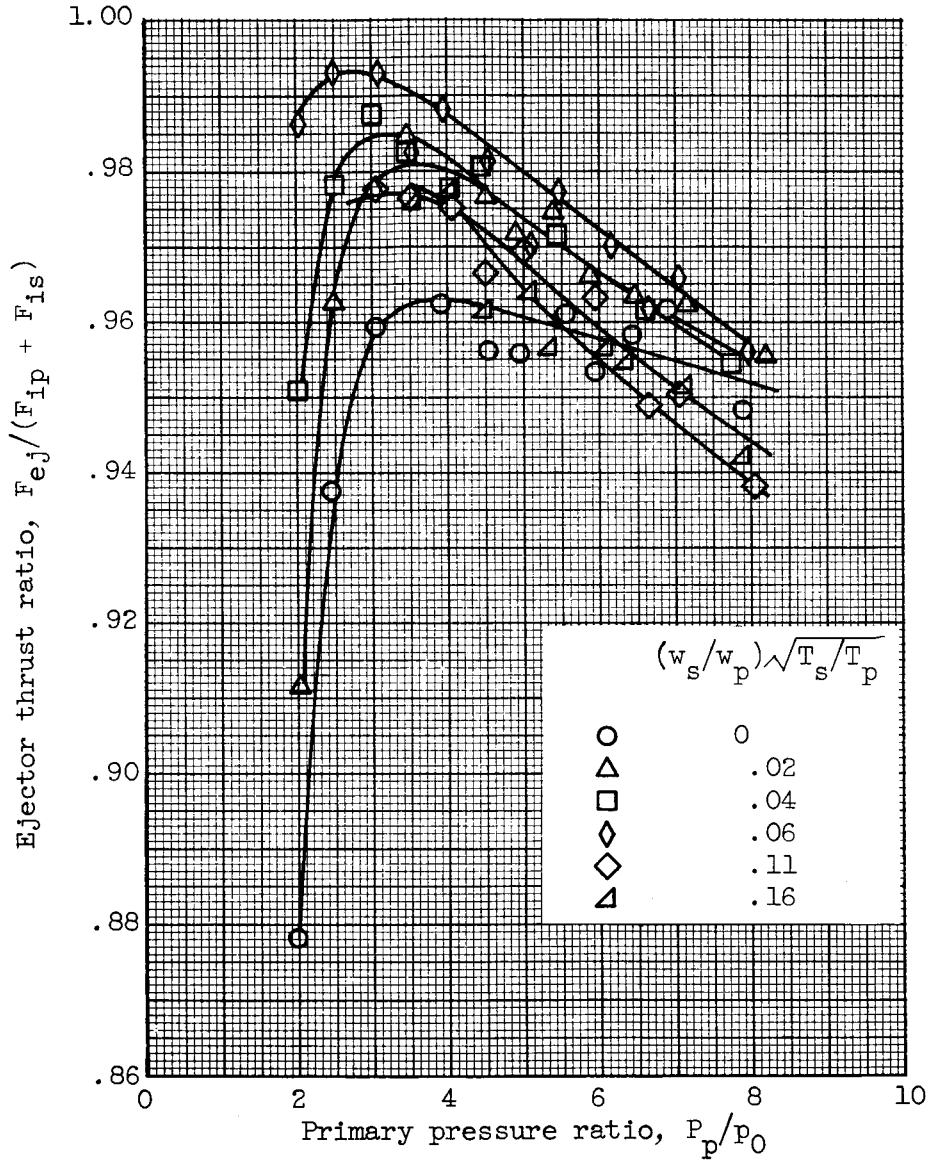

(a) Thrust performance.

Figure 13. - Ejector performance for configuration 8, which simulates position for nonafterburning, sea-level static.

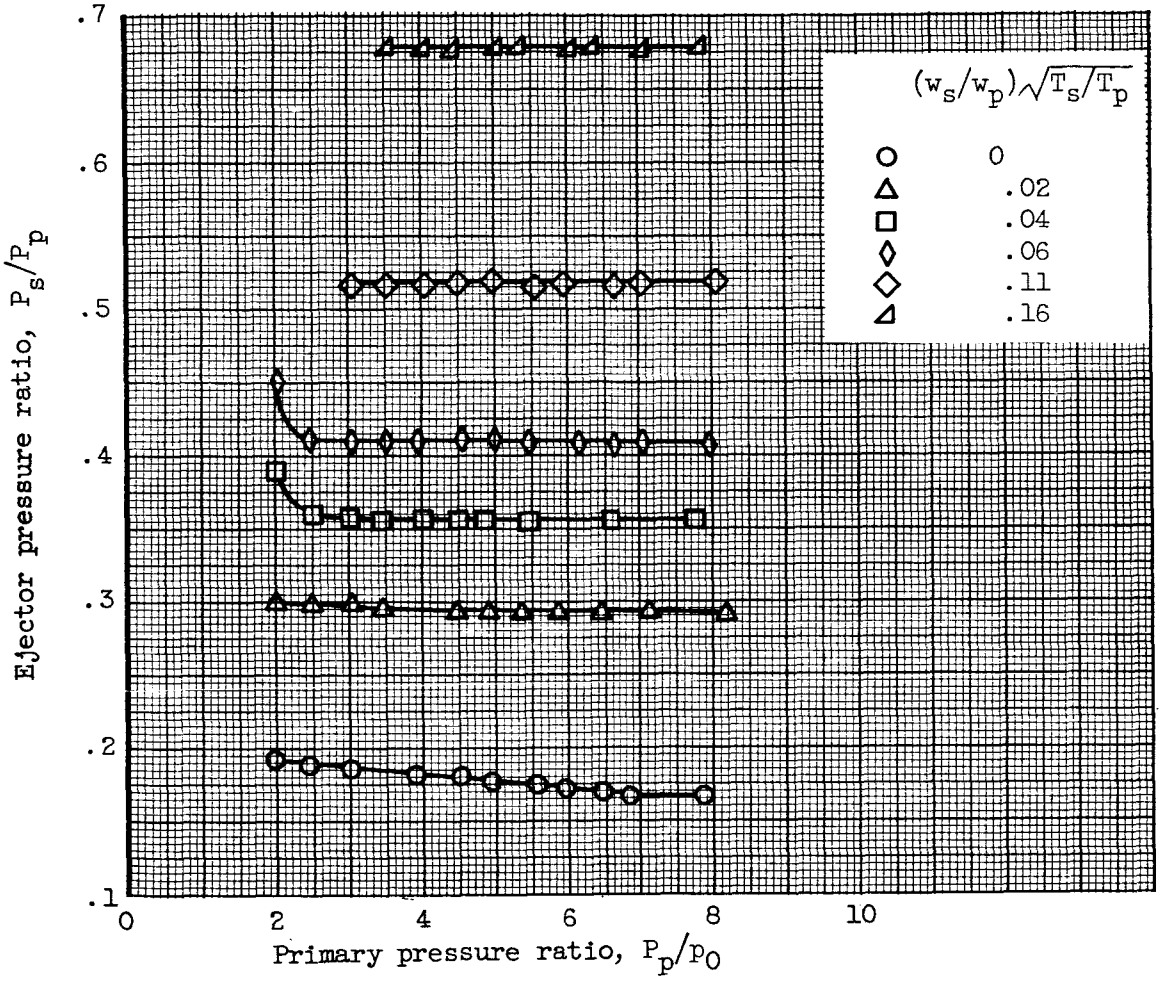

(b) Pumping performance.

Figure 13. - Concluded. Ejector performance for configuration 8, which simulates position for nonafterburning, sea-level static.

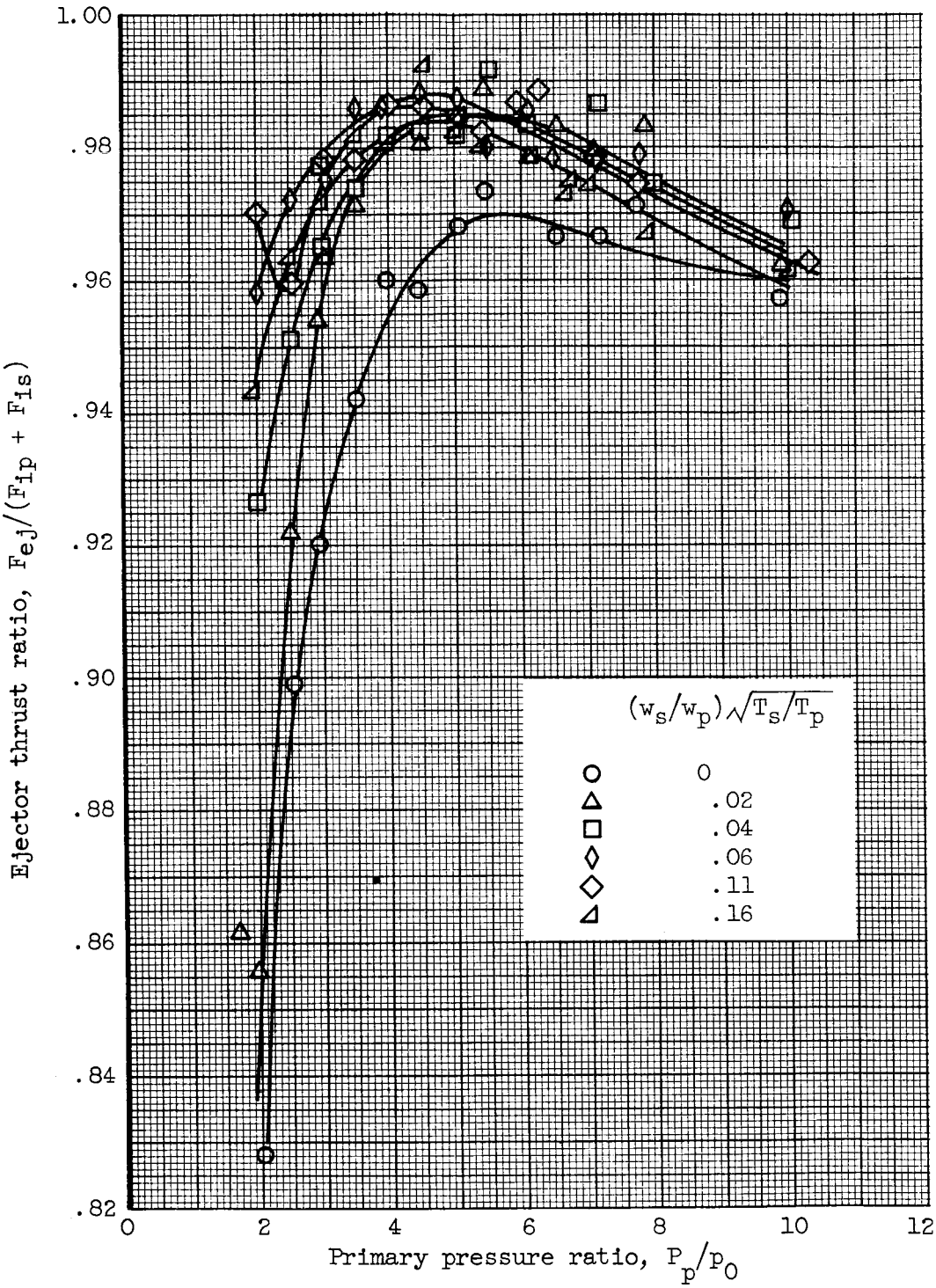

(a) Thrust performance.

Figure 14. - Ejector performance for configuration 9, which simulates position for nonafterburning, Mach 0.9.

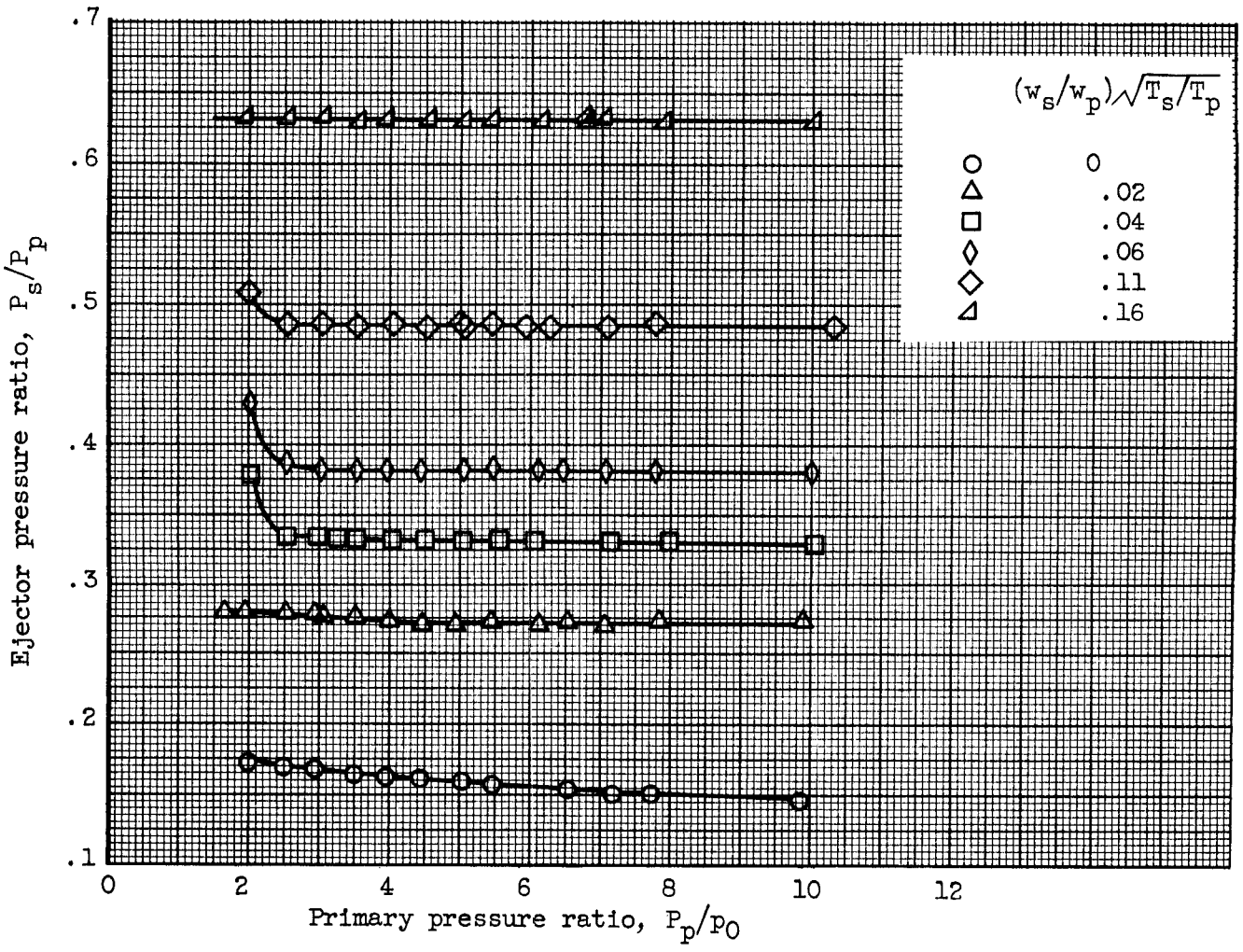

(b) Pumping performance.

Figure 14. - Concluded. Ejector performance for configuration 9, which simulates position for nonafterburning, Mach 0.9.

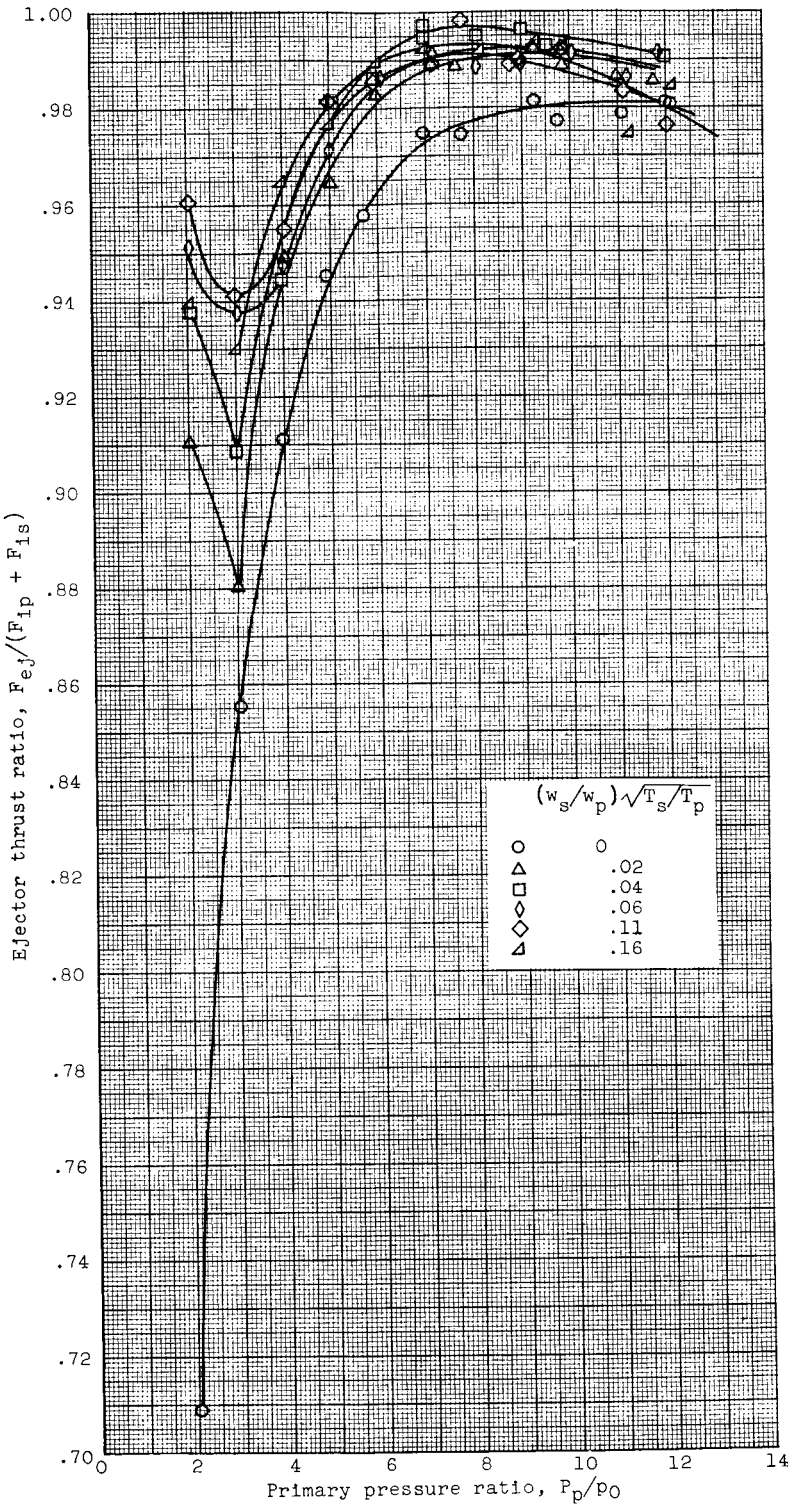

(a) Thrust performance.

Figure 15. - Ejector performance for configuration 10, which simulates position for nonafterburning, Mach 1.5.

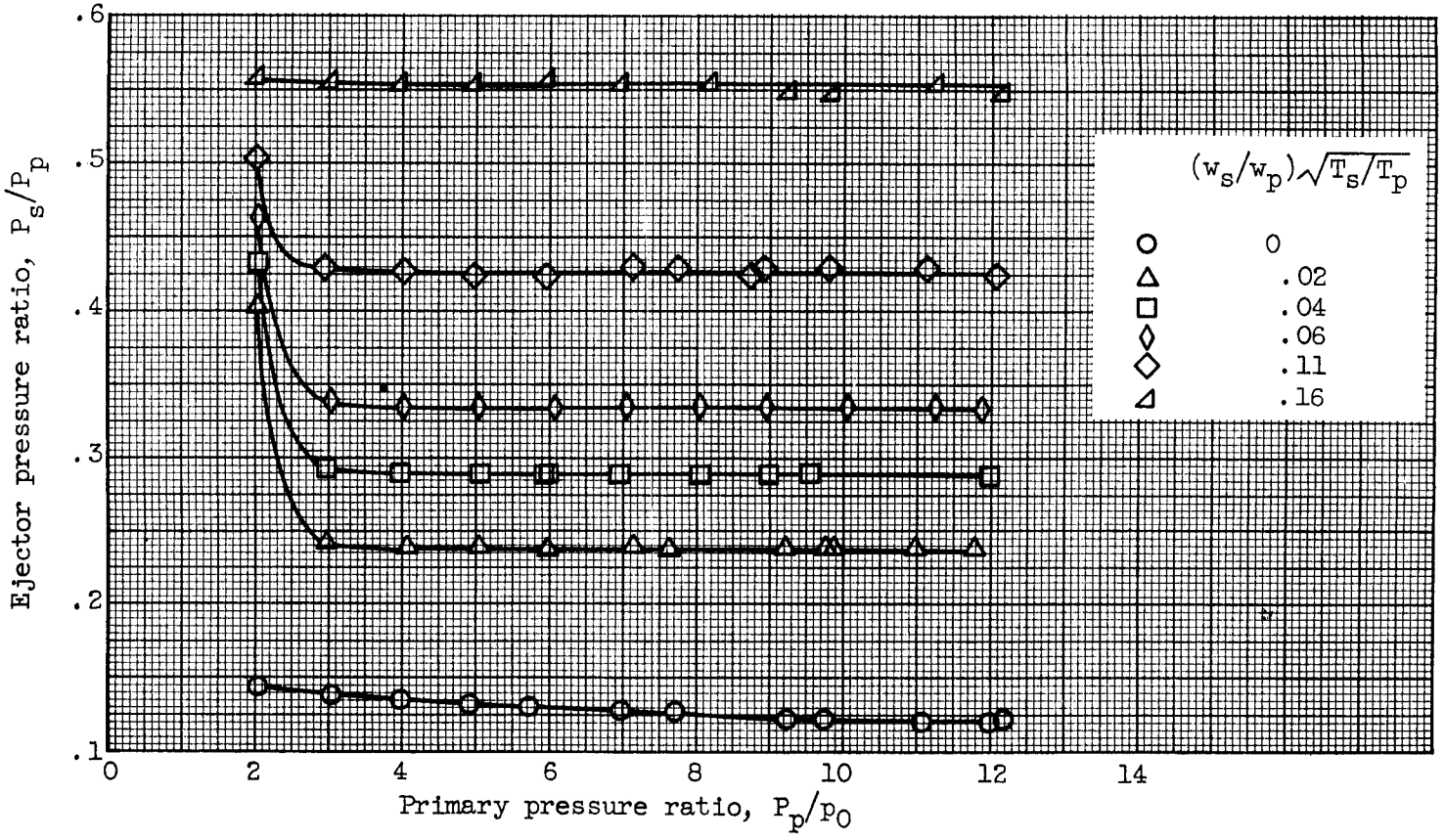

(b) Pumping performance.

Figure 15. - Concluded. Ejector performance for configuration 10, which simulates position for nonafterburning, Mach 1.5.

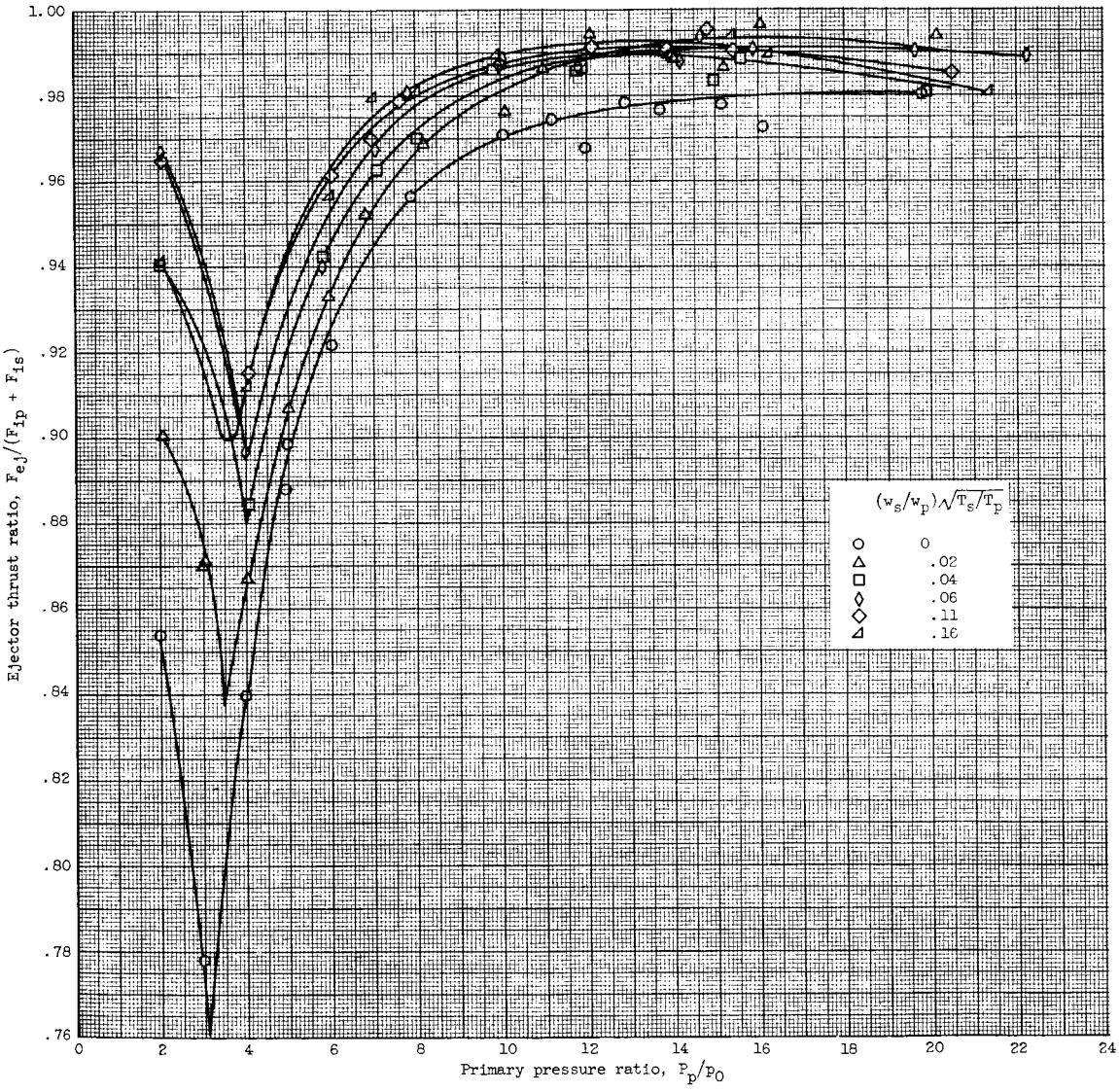

(a) Thrust performance.

Figure 16. - Ejector performance for configuration 11, which simulates position for nonafterburning. Mach 2.2.

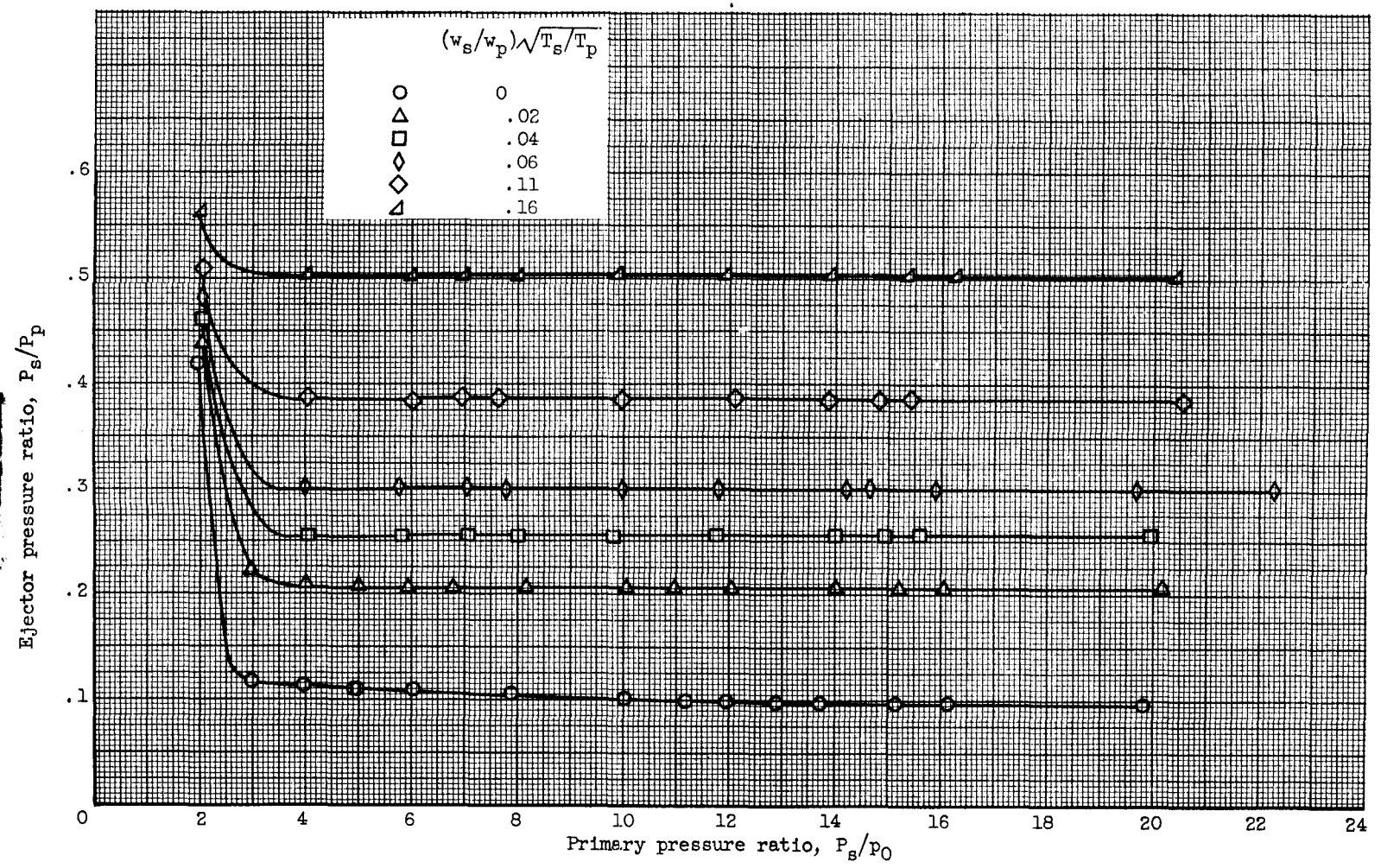

(b) Pumping performance.

Figure 16. - Concluded. Ejector performance for configuration 11, which simulates position for nonafterburning, Mach 2.2.

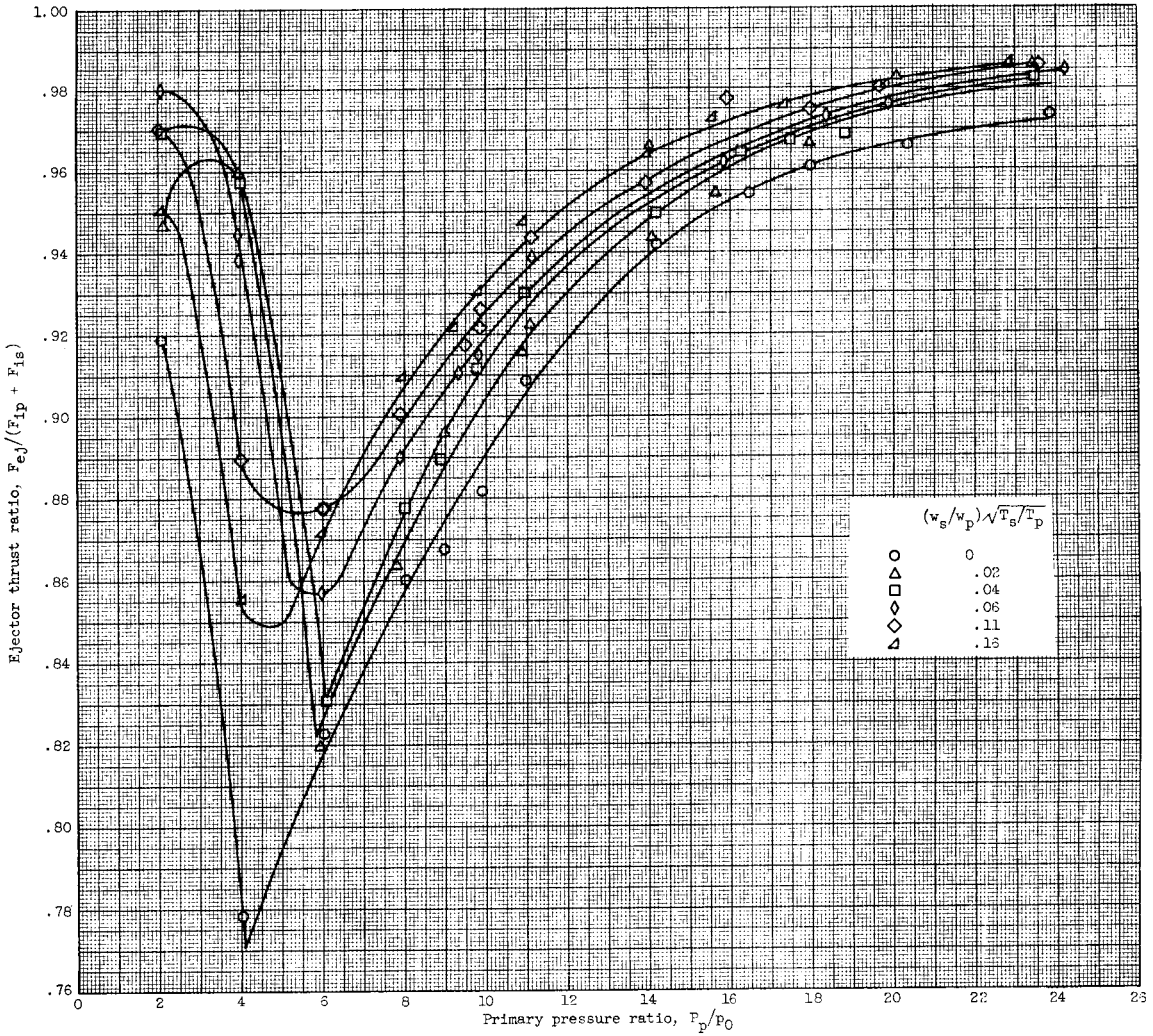

(a) Thrust performance.

Figure 17. - Ejector performance for configuration 12, which simulates position for nonafterburning. Mach 3.0.

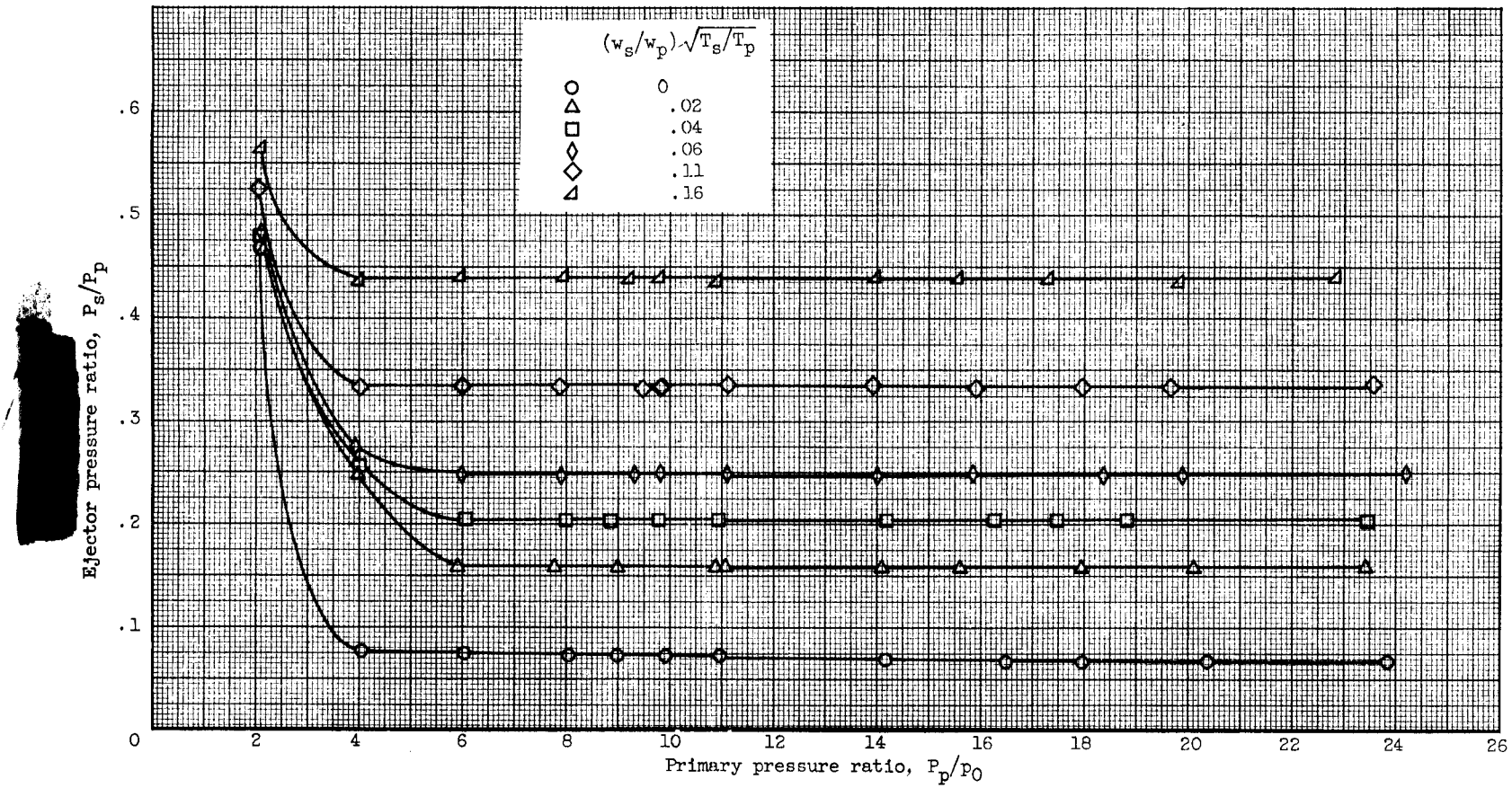

(b) Pumping performance.

Figure 17. - Concluded. Ejector performance for configuration 12, which simulates position for nonafterburning, Mach 3.0.

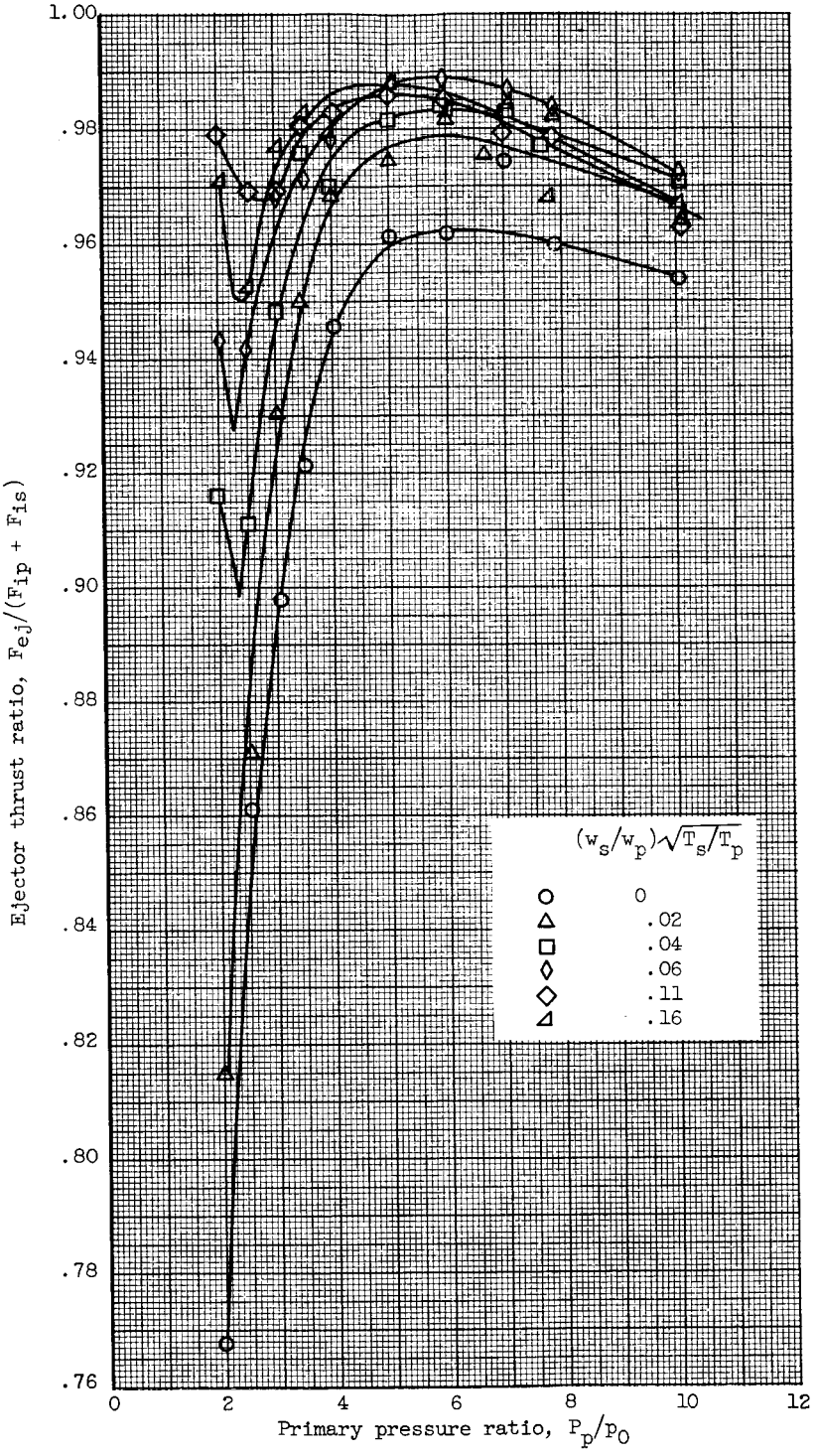

(a) Thrust performance.

Figure 18. - Ejector performance for configuration 13, which simulates position for nonafterburning, Mach 0.9 with 30 percent increase in gap height.

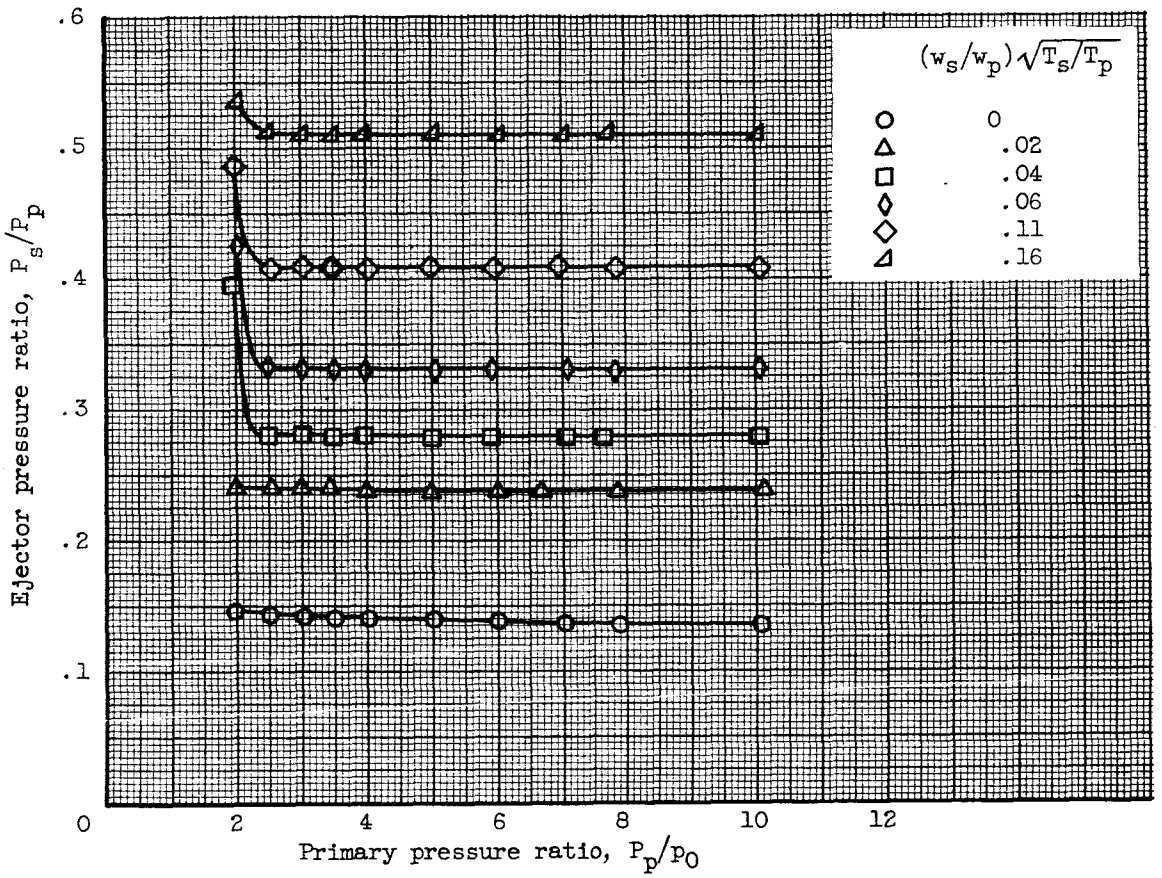

(b) Pumping performance.

Figure 18. - Concluded. Ejector performance for configuration 13, which simulates position for nonafterburning, Mach 0.9 with 30 percent increase in gap height.

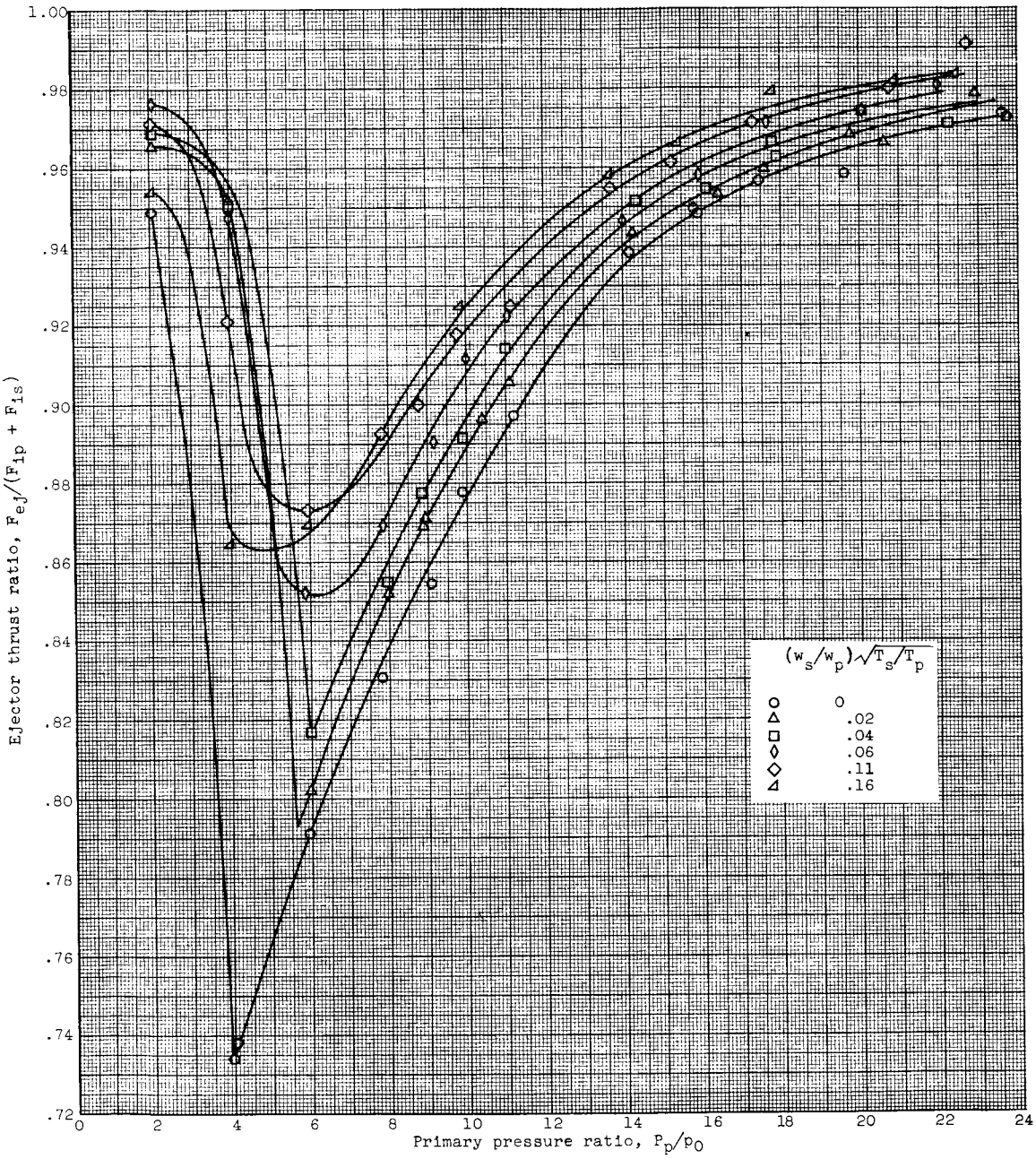

(a) Thrust performance.

Figure 19. - Ejector performance for configuration 14, which simulates position for nonafterburning, Mach 3.0 with 30 percent increase in gap height.

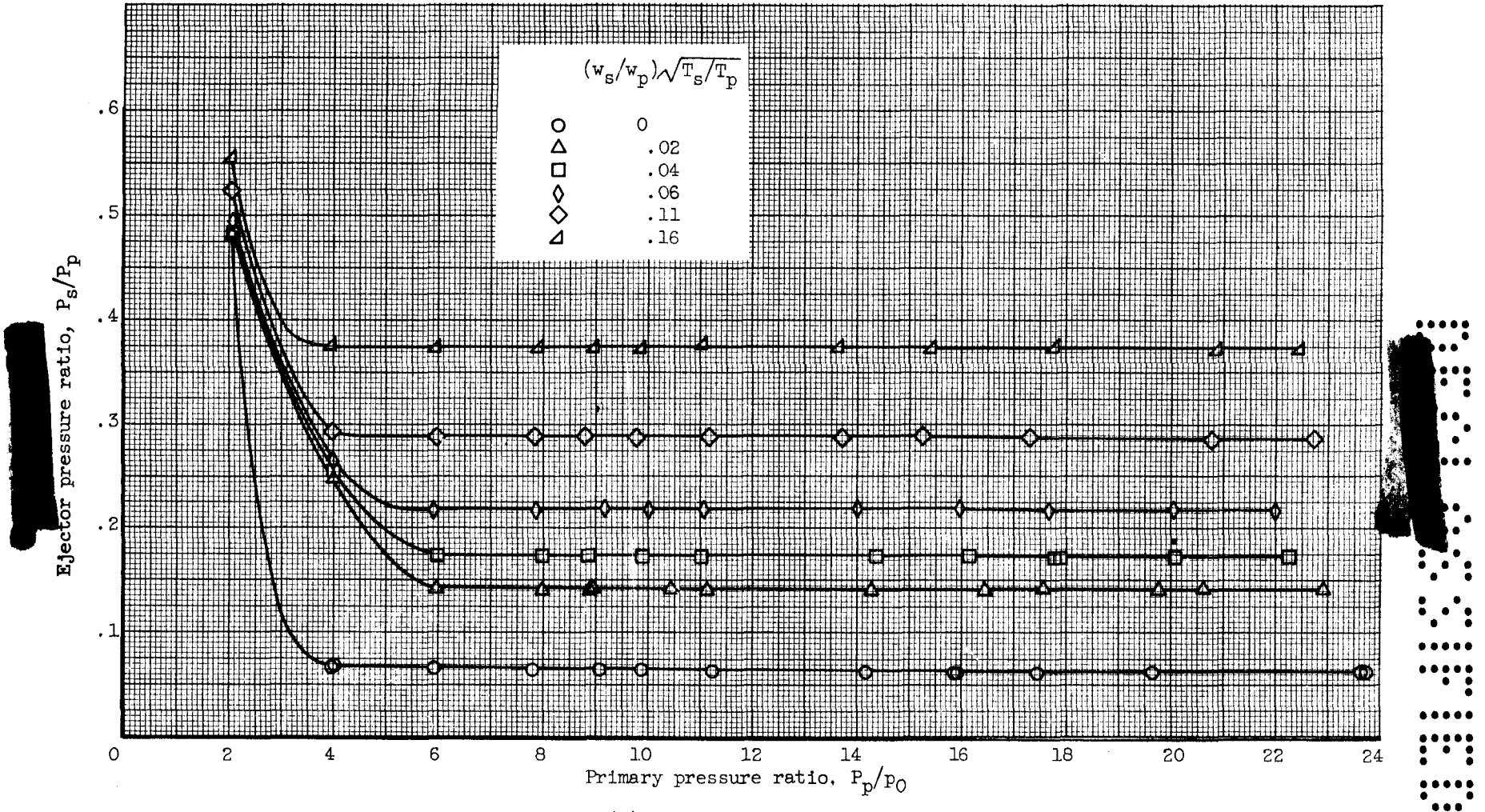

(b) Pumping performance.

Figure 19. - Concluded. Ejector performance for configuration 14, which simulates position for nonafterburning, Mach 3.0 with 30 percent increase in gap height.

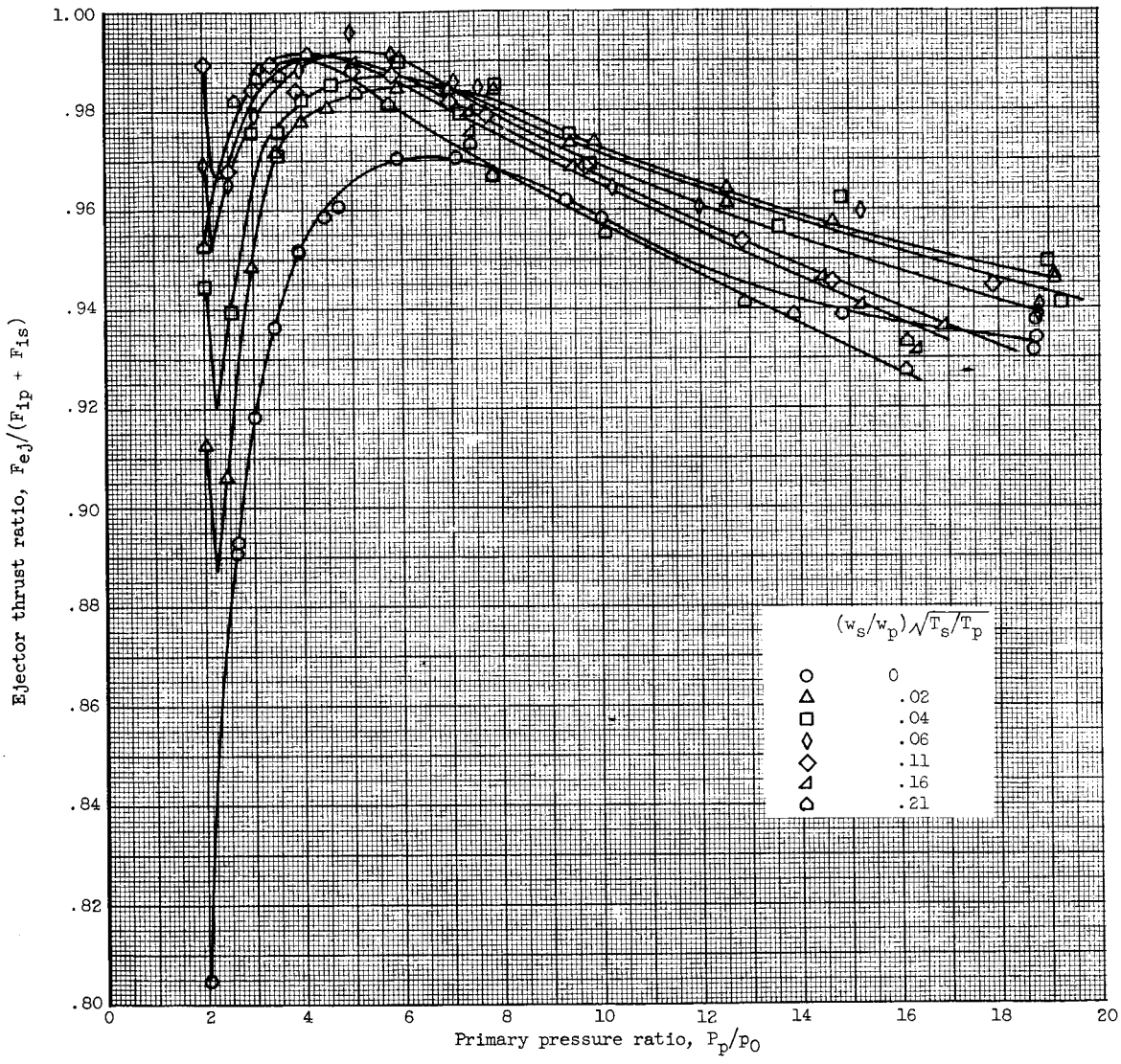

(a) Thrust performance.

Figure 20. - Ejector performance for configuration 15, which simulates position for maximum afterburning, Mach 0.9 with 30 percent increase in gap height.

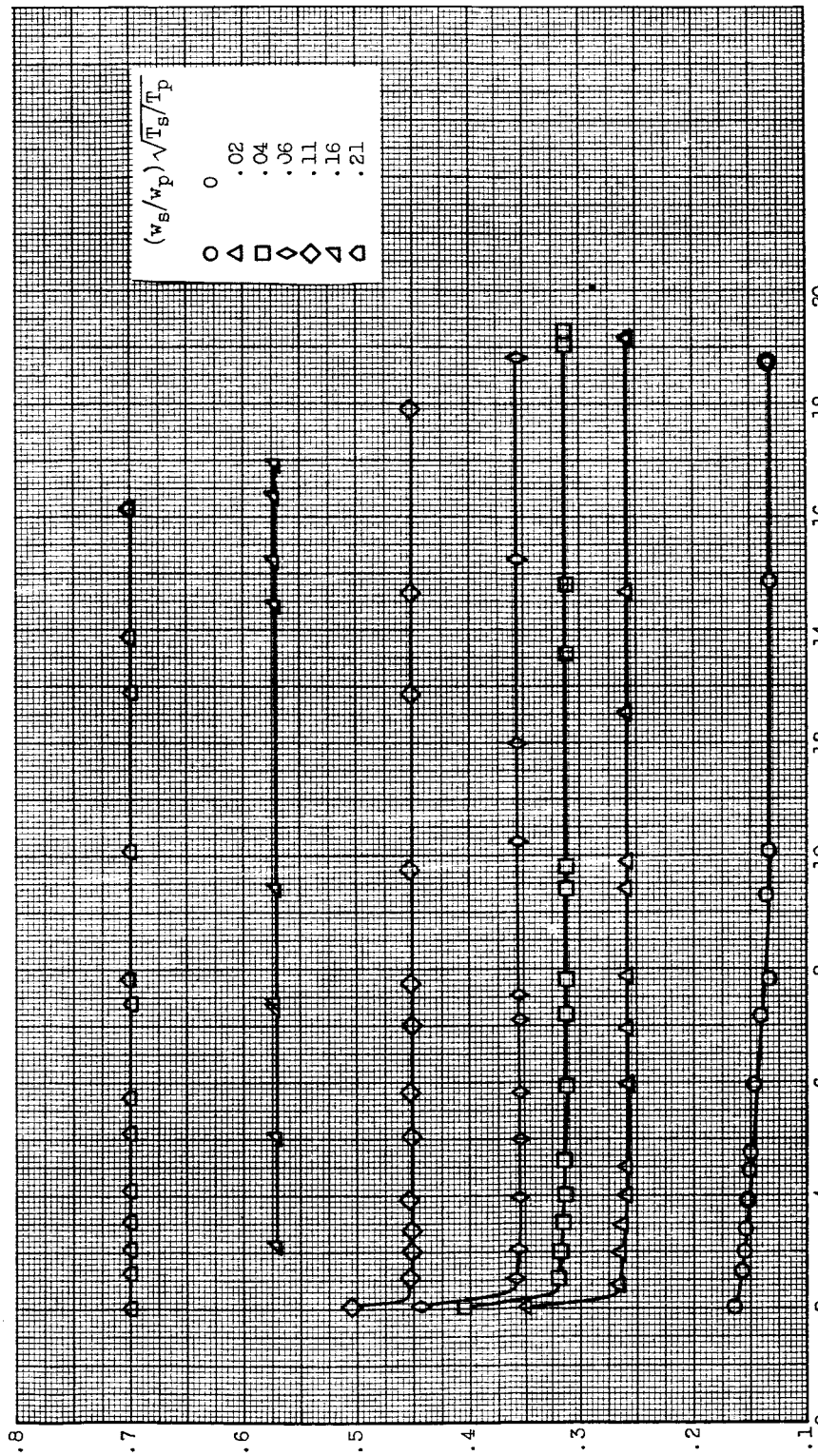

(b) Pumping performance.

Figure 20. - Concluded. Ejector performance for configuration 15, which simulates position for maximum afterburning, Mach 0.9 with 30 percent increase in gap height.

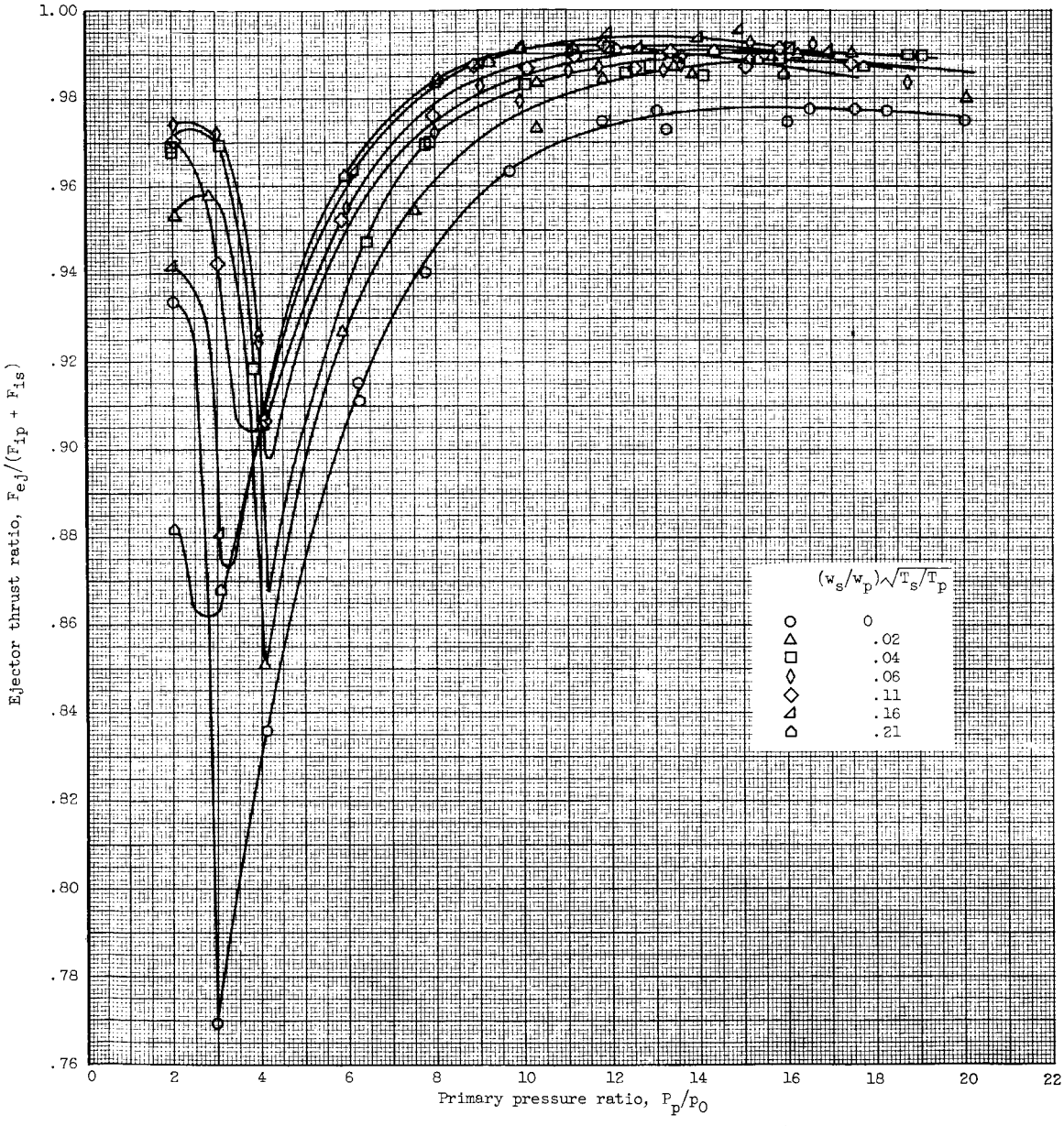

(a) Thrust performance.

Figure 21. - Ejector performance for configuration 16, which simulates position for maximum afterburning, Mach 2.2 with 30 percent increase in gap height.

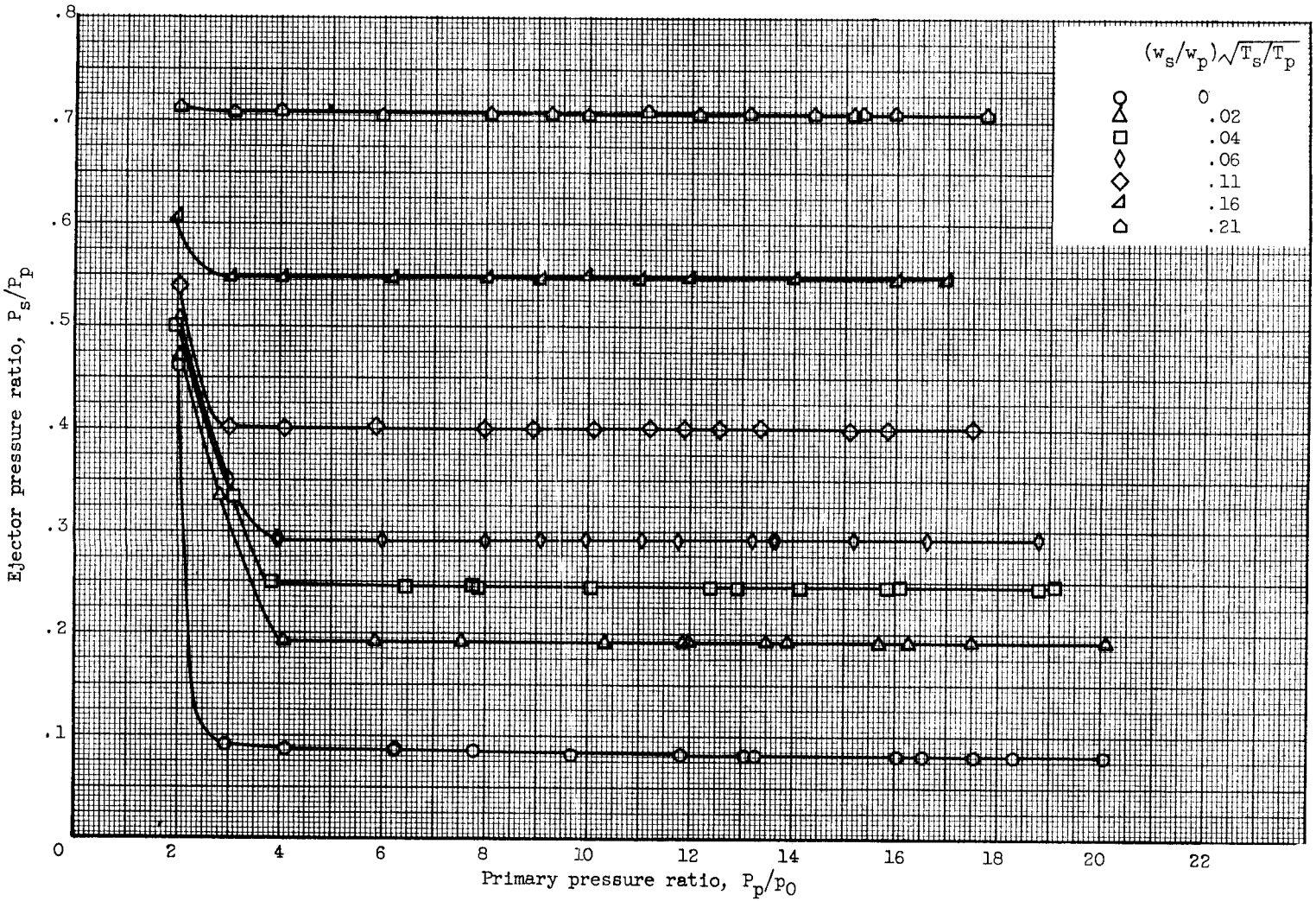

(b) Pumping performance.

Figure 21. - Concluded. Ejector performance for configuration 16, which simulates position for maximum afterburning, Mach 2.2 with 30 percent increase in gap height.

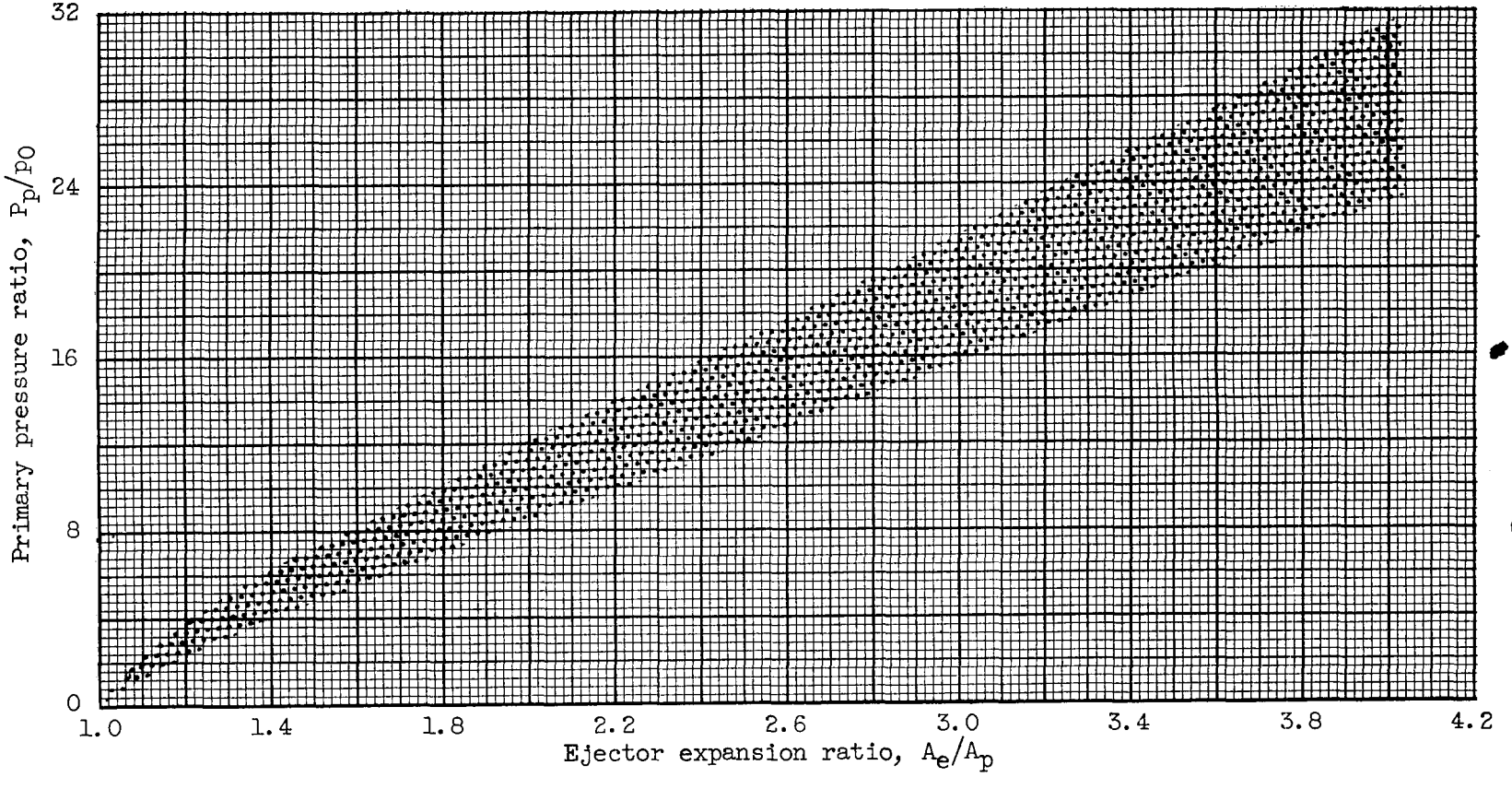

Figure 22. - Region where thrust ratio is within 1/4 percent of maximum value.

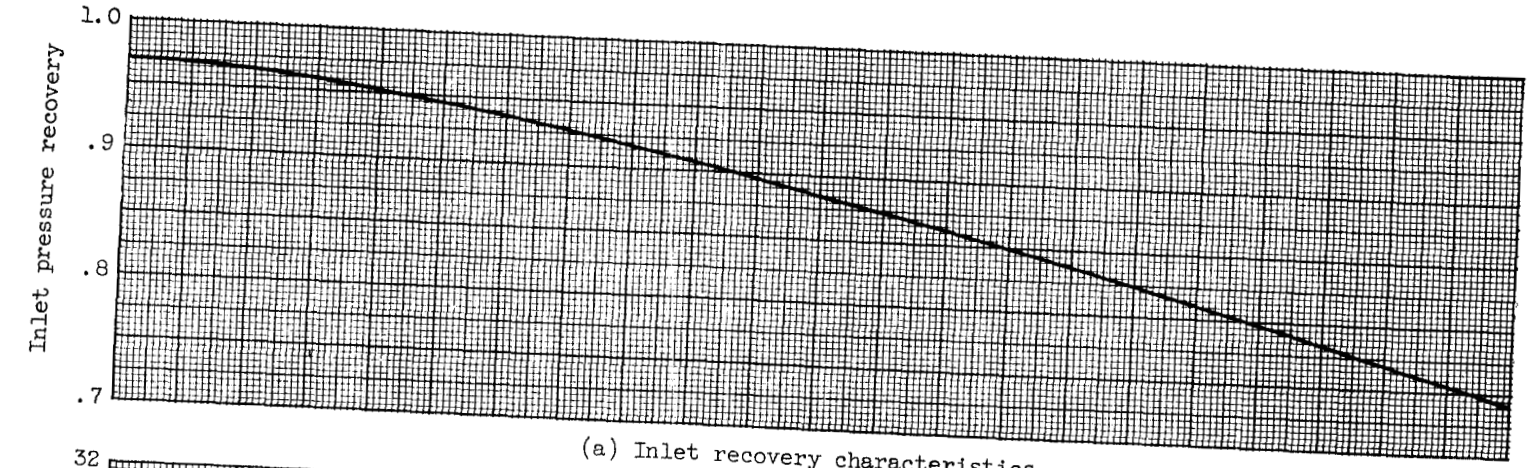

(a) Inlet recovery characteristics.

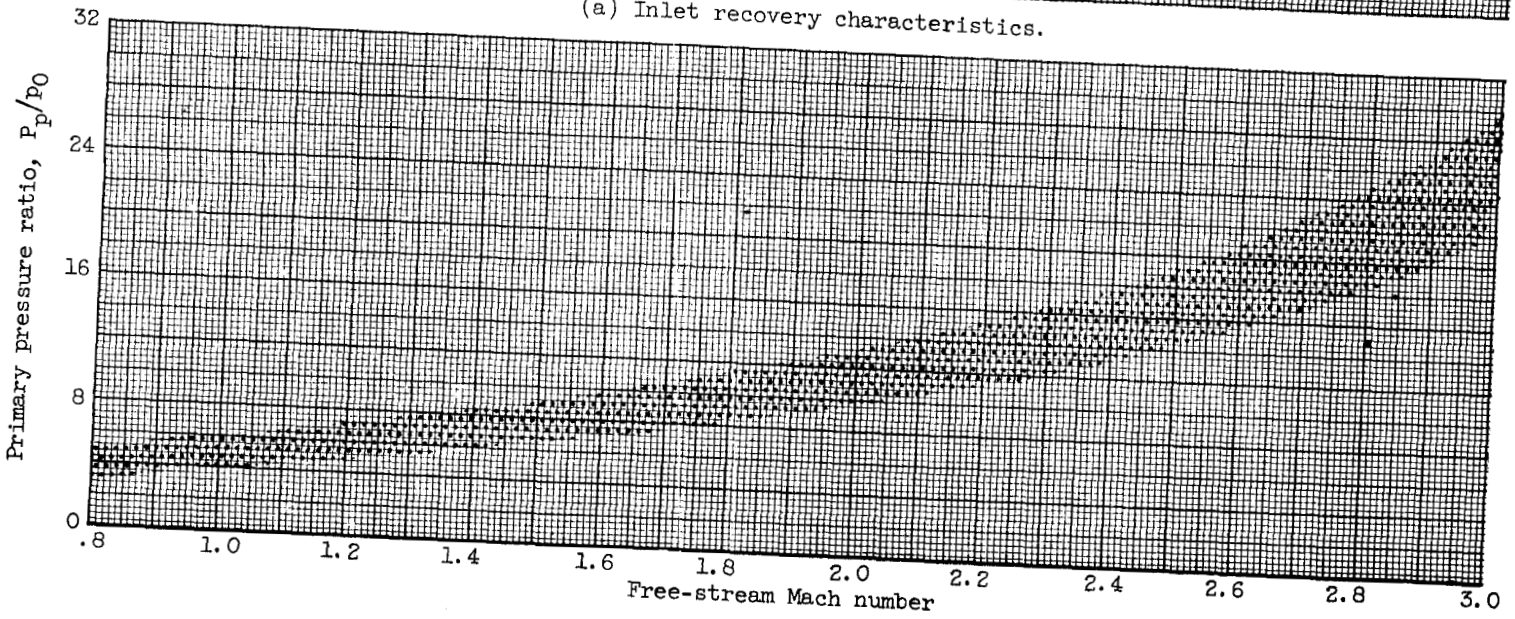

(b) Engine pressure-ratio schedule.

Figure 23. - Assumed engine operating schedule and inlet performance.

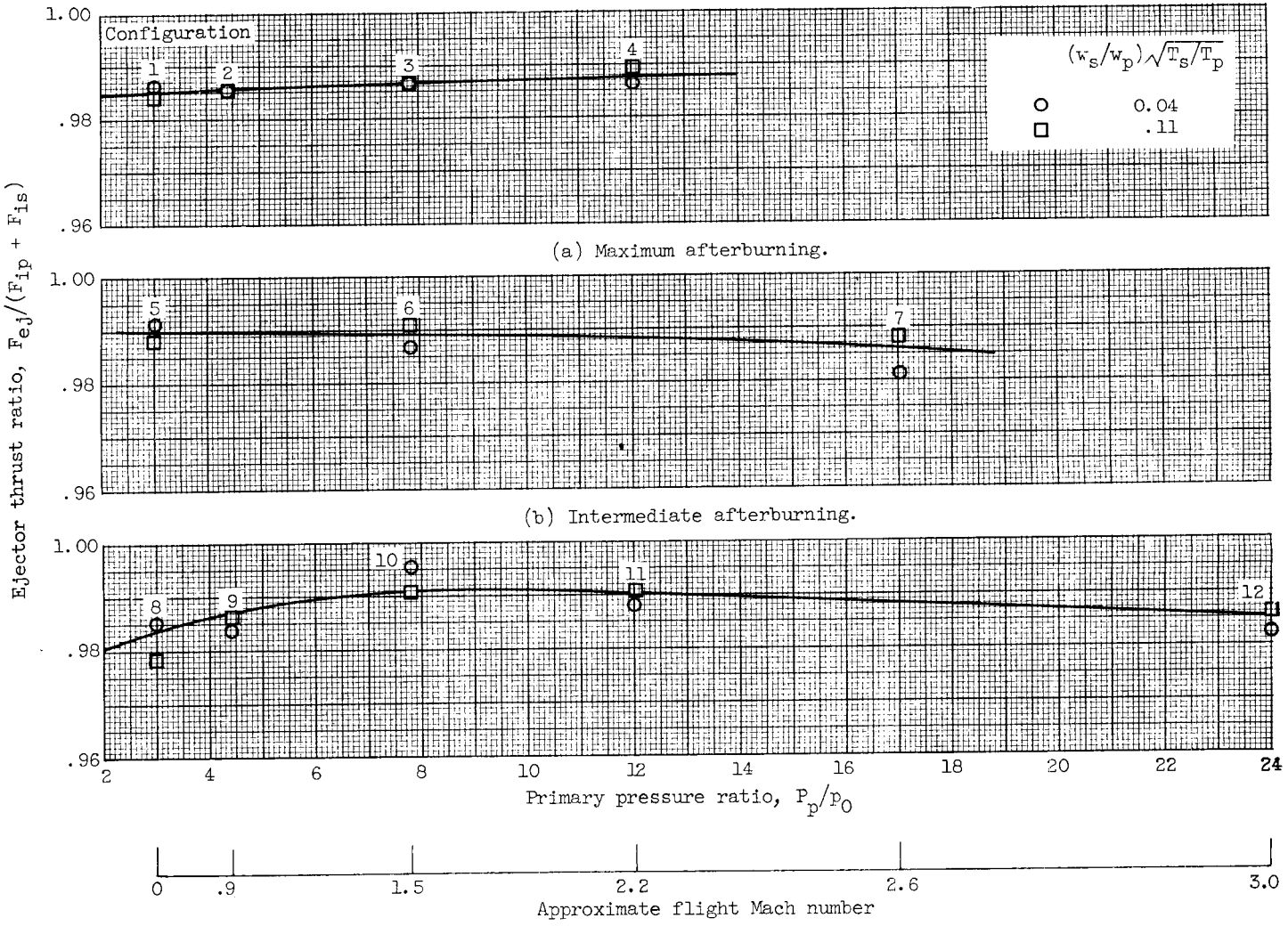

(a) Maximum afterburning.

(b) Intermediate afterburning.

(c) Nonafterburning.

Figure 24. - Composite thrust performance.

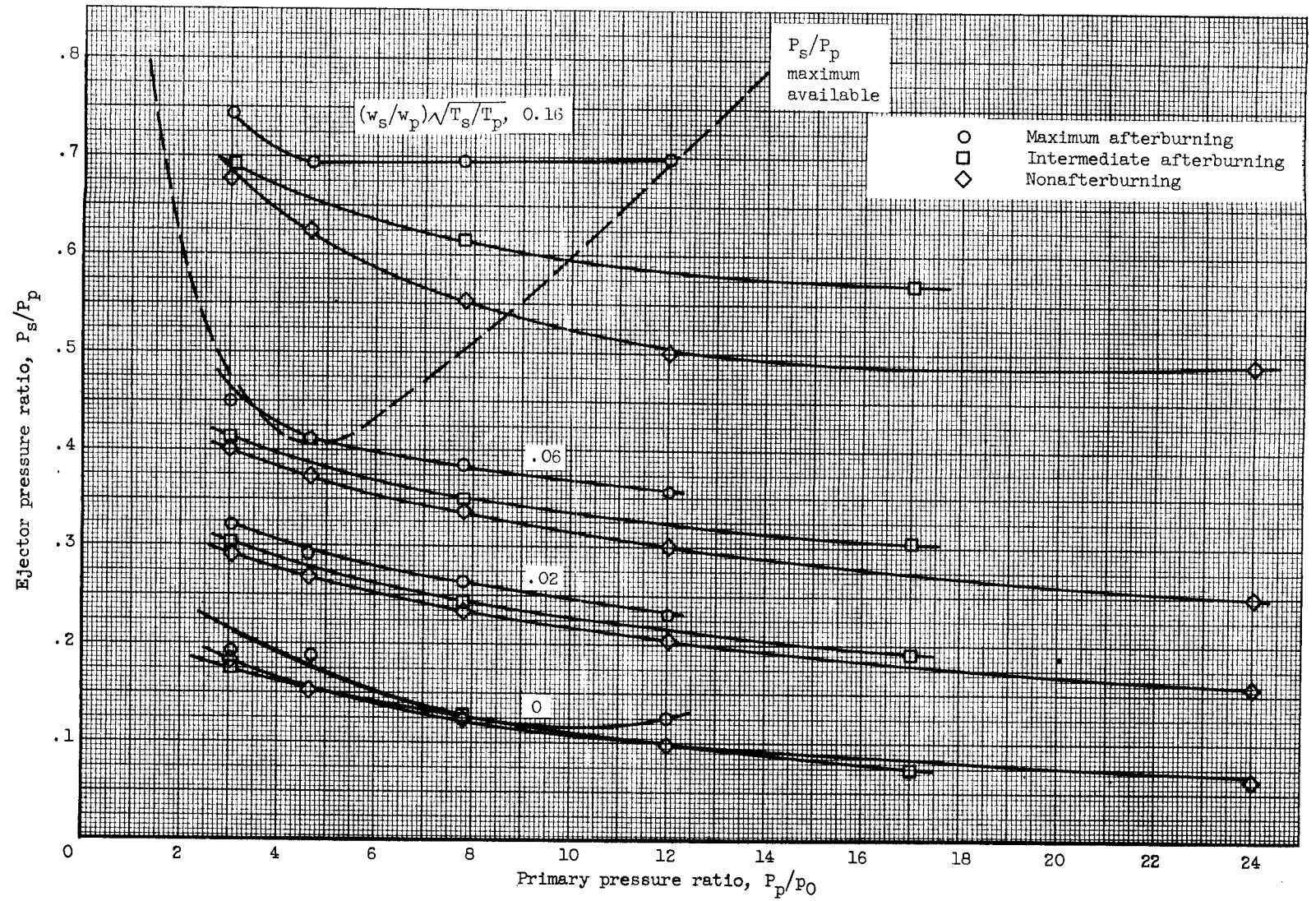

Figure 25. - Composite pumping performance.

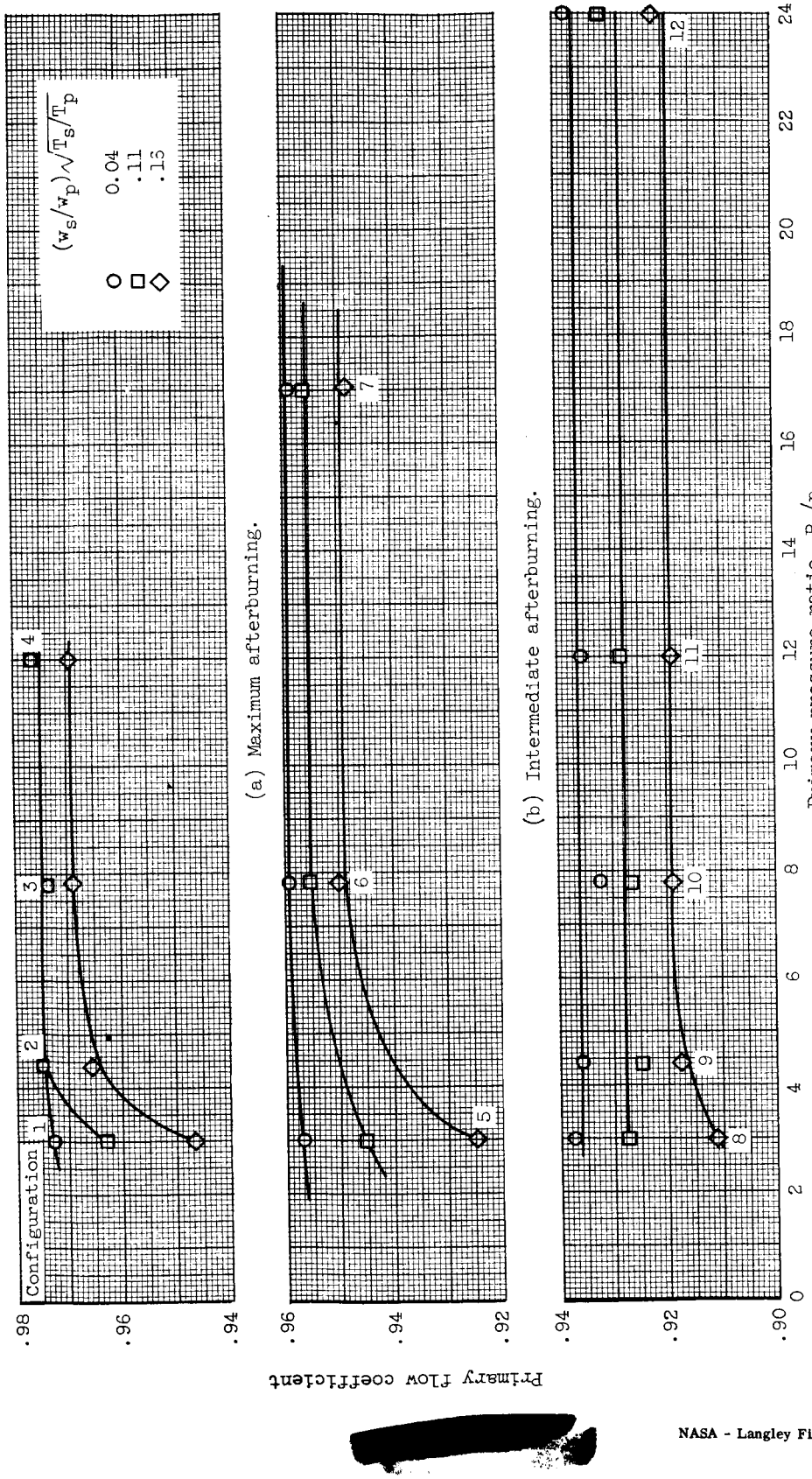

(a) Maximum afterburning.

(b) Intermediate afterburning.

(c) Nonafterburning.

Figure 26. - Composite primary-nozzle flow performance (with shrouds).

E-736